SIAM J. APPLIED DYNAMICAL SYSTEMS
Vol. 11, No. 4, pp. 1723–1753

Computer Assisted Existence Proofs of Lyapunov Orbits at L_2 and Transversal Intersections of Invariant Manifolds in the Jupiter–Sun PCR3BP*

Maciej J. Capiński†

Abstract. We present a computer assisted proof of existence of a family of Lyapunov orbits which stretches from L_2 (the collinear libration point between the primaries) up to half the distance to the smaller primary in the Jupiter–Sun planar circular restricted three body problem. We then focus on a small family of Lyapunov orbits with energies close to comet Oterma and show that their associated invariant manifolds intersect transversally. Our computer assisted proof provides explicit bounds on the location and on the angle of intersection.

Key words. invariant manifolds, restricted three body problem, cone conditions, parameterization method, computer assisted proofs

AMS subject classifications. 37D10, 37N05, 34C20, 34C45, 70F07, 70F15

DOI. 10.1137/110847366

1. Introduction.

The planar circular restricted three body problem (PCR3BP) has been extensively studied throughout literature. The model has applications in space mission design [14, 15], explains symbolic dynamics phenomena observed in trajectories of comets [18], and can be used for the study of diffusion estimates [16, 17]. All of the above are associated with dynamics along invariant manifolds of the system. In this paper we discuss how existence of such manifolds can be proved within explicit bounds using rigorous computer assisted techniques.

We focus on dynamics associated with the fixed point L_2, its associated center manifold, and stable/unstable manifolds. The problem has been studied by Llibre, Martinez, and Simó [19], where, under appropriate conditions on parameters of the system, existence and intersections of such manifolds have been proved analytically. A similar mechanism was considered by Belbruno and Marsden in [3] to describe the hopping of the comets of Jupiter using the empirical notion of the weak stability boundary. Later, in the work of Koon et al. [18], invariant manifolds and their associated symbolic dynamics were used to numerically explain a peculiar trajectory of Jupiter's comet Oterma. Such symbolic dynamics has been proved using rigorous computer assisted computations by Wilczak and Zgliczyński [23, 24]. In recent papers of Belbruno, Gidea, and Topputo [4, 5] it is shown that the weak stability boundary method and the invariant manifold method coincide.

The work presented in this paper can be viewed as an extension of [23, 24]. Results in

*Received by the editors September 8, 2011; accepted for publication (in revised form) by D. Scheeres August 27, 2012; published electronically December 13, 2012. This work was initiated during a visit of the author to the University of Texas at Austin, sponsored by the Kościuszko Foundation. This work was supported by the Polish State Ministry of Science and Information Technology under grant N201 543238.

http://www.siam.org/journals/siads/11-4/84736.html

†Faculty of Applied Mathematics, AGH University of Science and Technology, 30-059 Kraków, Poland (mcapinsk@agh.edu.pl).

[23, 24] were obtained using purely topological arguments. They focus on homoclinic and heteroclinic tangle between periodic orbits, without the detection of the manifolds themselves or angles of their intersections. Here we address these issues.

In this paper we shall first present a method for detecting of families of Lyapunov orbits in the PCR3BP. It is designed as a tool for rigorous computer assisted proofs. We apply the method to obtain a family that spans up to half the distance between the fixed point L_2 and the smaller primary in the Jupiter–Sun system. This is our first main result, which is stated in Theorem 3.2. The method is based on a combination of the interval Newton method and the implicit function theorem.

We then consider a small family of Lyapunov orbits with energies close to the energy of the comet Oterma. We prove that the family is normally hyperbolic, and we give a tool for obtaining rigorous bounds for its unstable and stable fibers. The tool is based on a topological approach combined with a parameterization method. We then show how fibers can be propagated to prove transversal intersections between stable and unstable manifolds of Lyapunov orbits. We investigate an intersection associated with manifolds which span from the Lyapunov orbit and circle around the larger primary. We obtain explicit bounds on the location of intersection and also on its angle. This is the second main result of the paper, which is stated in Theorem 4.1.

Both methods which we propose are tailor-made for the PCR3BP. We make use of the preservation of energy and reversibility of the system. Thanks to this our rigorous bounds for the investigated manifolds are quite sharp.

For our method we also develop a more general tool which can be applied for the detection of unstable/stable manifolds of saddle-center fixed points. It is a generalization of the work of Zgliczyński [25]. This is the subject of section 6.

The paper is organized as follows. Section 2 includes preliminaries which give an introduction to the PCR3BP, computer assisted proofs, and the interval Newton method and introduce some notation. In section 3 we present a method for the detection of families of Lyapunov orbits and apply it to the Jupiter–Sun system. In section 4 we outline the results for the intersections of invariant manifolds, which are then proved throughout the remainder of the paper. In section 5 we show how to prove that Lyapunov orbits are hyperbolic and foliated by energy. In section 6 we give a topological tool for detection of unstable manifolds of saddle-center fixed points. The method is then combined with a parameterization method in section 7 to obtain rigorous bounds on the intersections of invariant manifolds. Sections 8 and 9 contain, respectively, closing remarks and the appendix.

2. Preliminaries.

2.1. The PCR3BP. In the planar circular restricted three body problem (PCR3BP) we consider the motion of a small massless particle under the gravitational pull of two larger bodies (which we shall refer to as *primaries*) of mass μ and $1-\mu$. The primaries move around the origin on circular orbits of period 2π on the same plane as the massless body. In this paper we shall consider the mass parameter $\mu = 0.0009537$, which corresponds to the rescaled mass of Jupiter in the Jupiter–Sun system.

The Hamiltonian of the problem is given by [1]

$$H(q,p,t) = \frac{p_1^2 + p_2^2}{2} - \frac{1-\mu}{r_1(t)} - \frac{\mu}{r_2(t)},$$

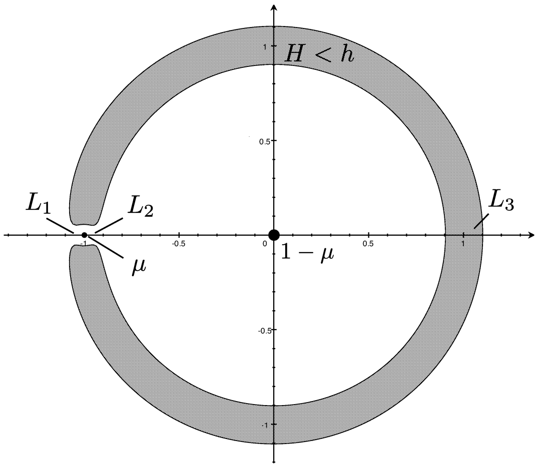

Figure 1. *The Hill's region for the energy level $h = 1.515$ of comet Oterma in the Jupiter–Sun system.*

where $(q, p) = (q_1, q_2, p_1, p_2)$ are the coordinates of the massless particle and $r_1(t)$ and $r_2(t)$ are the distances from the masses $1-\mu$ and μ, respectively.

After introducing a new coordinate system (x, y, p_x, p_y),

$$x = q_1 \cos t + q_2 \sin t, \qquad p_x = p_1 \cos t + p_2 \sin t,$$
$$y = -q_1 \sin t + q_2 \cos t, \qquad p_y = -p_1 \sin t + p_2 \cos t, \tag{2.1}$$

which rotates together with the primaries, the primaries become motionless (see Figure 1), and one obtains [1] an autonomous Hamiltonian

$$H(x, y, p_x, p_y) = \frac{(p_x + y)^2 + (p_y - x)^2}{2} - \Omega(x, y), \tag{2.2}$$

where

$$\Omega(x, y) = \frac{x^2 + y^2}{2} + \frac{1-\mu}{r_1} + \frac{\mu}{r_2},$$
$$r_1 = \sqrt{(x-\mu)^2 + y^2}, \qquad r_2 = \sqrt{(x + 1 - \mu)^2 + y^2}.$$

The motion of the particle is given by

$$\dot{q} = J\nabla H(q), \tag{2.3}$$

where $q = (x, y, p_x, p_y) \in \mathbb{R}^4$, $J = \left(\begin{smallmatrix} 0 & \mathrm{id} \\ -\mathrm{id} & 0 \end{smallmatrix}\right)$, and id is a two dimensional identity matrix.

The movement of the flow (2.3) is restricted to the hypersurfaces determined by the energy level h,

$$M(h) = \{(x, y, p_x, p_y) \in \mathbb{R}^4 | H(x, y, p_x, p_y) = h\}. \tag{2.4}$$

This means that movement in the x, y coordinates is restricted to the so-called Hill's region defined by

$$R(h) = \{(x, y) \in \mathbb{R}^2 | \Omega(x, y) \geq -h\}.$$

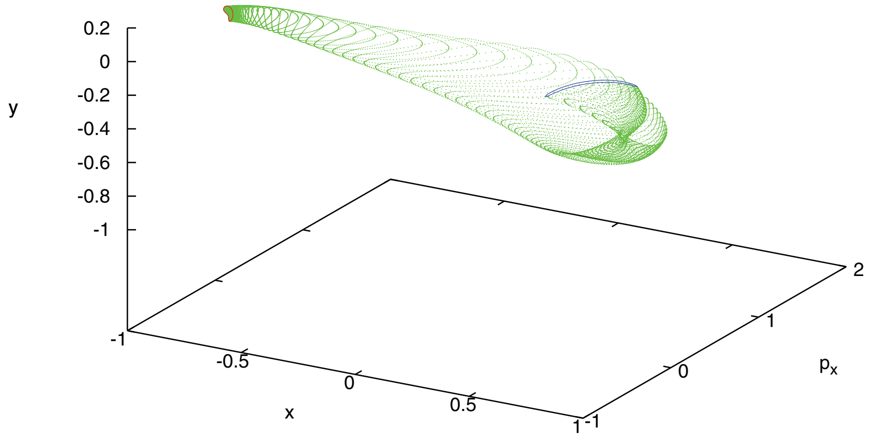

Figure 2. *The Lyapunov orbit in red, its unstable manifold in green, and the intersection of the unstable manifold with section $\{y = 0\}$ in blue, projected onto x, y, p_x coordinates. The figure is for the energy of comet Oterma $h = 1.515$ in the Jupiter–Sun system.*

The problem has three equilibrium points L_1, L_2, L_3 on the x-axis (see Figure 1). We shall be interested in the dynamics associated with L_2 and with orbits of energies higher than that of L_2. The linearized vector field at the point L_2 has two real and two purely imaginary eigenvalues; thus by the Lyapunov theorem (see, for example, [19]) for energies h larger and sufficiently close to $H(L_2)$ there exists a family of periodic orbits parameterized by energy emanating from the equilibrium point L_2. Numerical evidence shows that this family extends up to and even beyond the smaller primary μ [6].

The PCR3BP admits the following reversing symmetry:

$$S(x, y, p_x, p_y) = (x, -y, -p_x, p_y).$$

For the flow $\phi(t, q)$ of (2.3) we have

$$S(\phi(t, q)) = \phi(-t, S(q)). \tag{2.5}$$

We say that an orbit $q(t)$ is S-symmetric when

$$S(q(t)) = q(-t). \tag{2.6}$$

Each Lyapunov orbit is S-symmetric. It possesses a two dimensional stable manifold and a two dimensional unstable manifold. These manifolds lie on the same energy level as the orbit, and their intersection, when restricted to the three dimensional constant energy manifold (2.4), is transversal. These invariant manifolds are S-symmetric with respect to each other, meaning that the stable manifold is an image by S of the unstable manifold (see Figure 2 for the unstable manifold and Figure 3 for the intersection of manifolds). All these facts are well known and extensively studied numerically.

Our aim in this paper will be first to provide a rigorous computer assisted proof of existence of the manifold of Lyapunov orbits over a large radius from L_2 (see Figure 4). Second, using rigorous computer assisted computations, we shall show that for orbits with energies close to

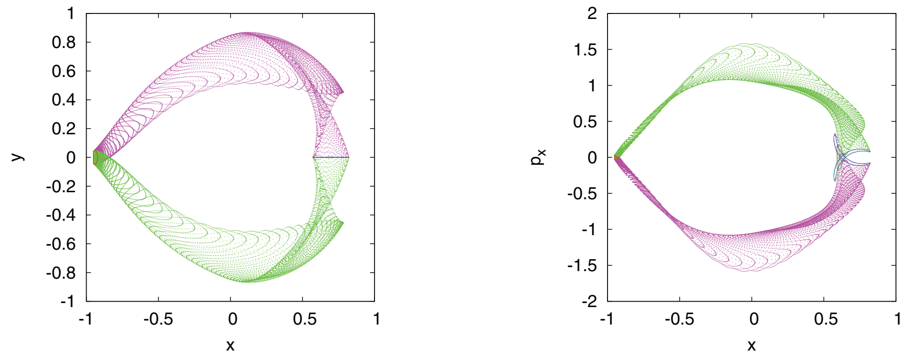

Figure 3. *The Lyapunov orbit in red, its unstable manifold in green, stable manifold in purple, and their intersections with section $\{y = 0\}$ in blue, projected onto x, y coordinates (left) and x, p_x coordinates (right). The figure is for the energy of comet Oterma $h = 1.515$ in the Jupiter–Sun system.*

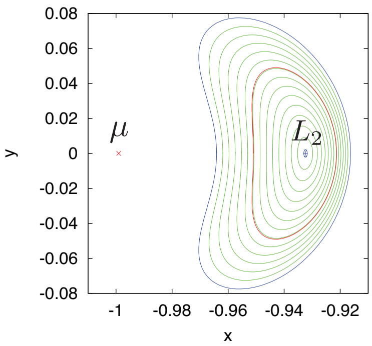

Figure 4. *The considered family of Lyapunov orbits in green (spanning between two orbits in blue), together with the Lyapunov orbit for the energy of the comet Oterma $h = 1.515$ in red.*

the energy of comet Oterma $h = 1.515$ their associated stable and unstable manifolds intersect transversally. Even though such intersections are well known from numerical investigation, to the best of our knowledge this is the first rigorous proof of their existence.

2.2. Computer assisted proofs. Most computations performed on a computer are burdened with error. Even very simple operations on real numbers (such as adding, multiplying, or dividing) can result in truncation errors. To make computer assisted computations fully rigorous, one can employ interval arithmetic, where instead of real numbers one deals with intervals. Any operation is made rigorous by appropriate rounding, which ensures enclosure of the true result.

Interval arithmetic can also be used to treat basic functions (such as sin, cos, or exponent). It can be extended to perform linear algebra on interval vectors and interval matrices. One can thus design algorithms which give rigorous enclosures for multiplying matrices, inverting a matrix, computing eigenvectors, or solving linear equations.

The interval arithmetic approach can also be extended to treat functions $f : \mathbb{R}^n \to \mathbb{R}^m$. One can implement algorithms which compute interval enclosures for images of the function

f for its derivative and for higher order derivatives.

The interval arithmetic approach can also be used for the integration of ODEs. One can implement interval arithmetic based integrators, which allow for the computation of enclosures of the images of points along a flow of an ODE. One can extend such integrators to include the computation of high order derivatives of a time shift map along the flow, or even to compute high order derivatives for Poincaré maps [22].

All the above-mentioned tasks can be performed using the single `C++` library "Computer Assisted Proofs in Dynamics" (CAPD). The package is freely available at http://capd.ii.uj.edu.pl. All the computer assisted proofs in this paper have been performed using the CAPD package. In section 9.3 we give more detailed comments on the modules of the CAPD library, which were required for our computations.

2.3. Interval Newton method. Let X be a subset of $\mathbb{R}^n$. We shall denote by $[X]$ an interval enclosure of the set X, that is, a set

$$[X] = \Pi_{i=1}^{n}[a_i, b_i] \subset \mathbb{R}^n,$$

such that

$$X \subset [X].$$

Let $f : \mathbb{R}^n \to \mathbb{R}^n$ be a C^1 function and $U \subset \mathbb{R}^n$. We shall denote by $[Df(U)]$ the interval enclosure of a Jacobian matrix on the set U. This means that $[Df(U)]$ is an interval matrix defined as

$$[Df(U)] = \left\{ A \in \mathbb{R}^{n\times n} | A_{ij} \in \left[\inf_{x\in U} \frac{df_i}{dx_j}(x), \sup_{x\in U} \frac{df_i}{dx_j}(x) \right] \text{ for all } i, j = 1, \dots, n \right\}.$$

Theorem 2.1 (interval Newton method [2]). *Let $f : \mathbb{R}^n \to \mathbb{R}^n$ be a C^1 function and $X = \Pi_{i=1}^{n}[a_i, b_i]$ with $a_i < b_i$. If $[Df(X)]$ is invertible and there exists an x_0 in X such that*

$$N(x_0, X) := x_0 - [Df(X)]^{-1} f(x_0) \subset X,$$

then there exists a unique point $x^* \in X$ such that $f(x^*) = 0$.

2.4. Notation. Throughout the paper we shall use the notation $\phi(t, x)$ for the flow and $\Phi_T(x) = \phi(T, x)$ for a time T shift along trajectory map of (2.3). For points $p = (x, y)$ we shall write $\pi_x p$ and $\pi_y p$ to denote projections onto coordinates x and y, respectively. We shall also use the following notation for a Cartesian product of sets $\Pi_{i=1}^{n} U_i = U_1 \times \cdots \times U_n$. For $A, B \subset \mathbb{R}^n$ we use the notation $A + B = \{a + b | a \in A, b \in B\}$.

3. Existence of a family of Lyapunov orbits. In this section we present a method for proving the existence of Lyapunov orbits far away from L_2. The result is in the spirit of the method applied by Wilczak and Zgliczyński in [23, 24] for a Lyapunov orbit with energy $h = 1.515$ of the comet Oterma. Our result differs from [23, 24] in that we obtain a smooth family of orbits over a large set, whereas in [23, 24] a single orbit was proved.

We shall consider orbits starting from points of the form $(x, 0, 0, p_y)$ with x inside of an interval

$$I_x = [\underline{I_x}, \overline{I_x}] := \left[\frac{1}{2}(-1 + \mu - 0.933), -0.933 \right] \tag{3.1}$$
$$\approx [-0.96602315, -0.933] \subset \mathbb{R}.$$

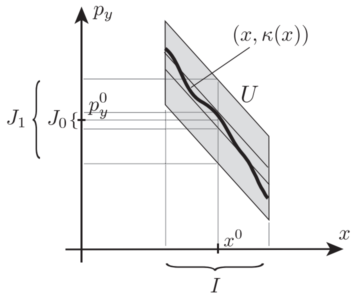

Figure 5. *The bound for a curve of points $q(x) = (x, 0, 0, \kappa(x))$ on Lyapunov orbits.*

Since $\pi_x L_2 \approx -0.93237$, we see that $\underline{I_x} < \frac{1}{2}(-1 + \mu - \pi_x L_2)$, so the interval I_x stretches from half the distance between the smaller primary and L_2 almost up to L_2 (see Figure 4, where the orbits are depicted in green and stretch between an inner and outer orbit depicted in blue).

Let us consider a section $\Sigma = \{y = 0\}$ and a Poincaré map $P : \Sigma \to \Sigma$ of (2.3). We shall interpret the Poincaré map as a function from $\mathbb{R}^3$ to $\mathbb{R}^3$ with coordinates x, p_x, p_y. If for a point $q = (x, 0, p_y) \in \Sigma$ we have $\pi_{p_x} P(q) = 0$, then by the symmetry property (2.5) the point q lies on a periodic orbit (the Poincaré map P makes a half turn along the orbit starting from q).

Let us introduce the following notation:

$$f : \mathbb{R}^2 \to \mathbb{R},$$
$$f(x, p_y) = \pi_{p_x} P(x, 0, p_y).$$

To find a periodic orbit for some fixed x it is sufficient to find a zero of a function

$$g_x(p_y) := f(x, p_y).$$

Let $DP = (dP_{i\,j})_{i,j=1,2,3}$ be the derivative of the map P, with indexes $1, 2, 3$ corresponding to coordinates x, p_x, p_y, respectively.

Lemma 3.1. *Let I and J_i for $i = 0, 1$ be closed intervals such that J_0, J_1 have the same center point p_y^0 and $J_0 \subset J_1$. Let x^0 be the center point of I. Let $a \in \mathbb{R}$ and $U_0, U \subset \Sigma = \mathbb{R}^3$ be sets defined as (see Figure 5)*

$$U_0 = \{x^0\} \times \{0\} \times J_0,$$
$$U = \left\{(x, 0, p_y) | x \in I, p_y = a\left(x - x^0\right) + \iota, \iota \in J_1\right\}. \tag{3.2}$$

If

$$N := p_y^0 - \left[\frac{\pi_{p_x} P(x^0, 0, p_y^0)}{dP(U_0)_{2\,3}}\right] \subset J_0 \tag{3.3}$$

and

$$|\alpha - a| < \frac{1}{|I|}\left(|J_1| - |J_0|\right) \quad \textit{for all } \alpha \in [\underline{\alpha}, \overline{\alpha}] := \left[-\frac{dP(U)_{2\,1}}{dP(U)_{2\,3}}\right], \tag{3.4}$$

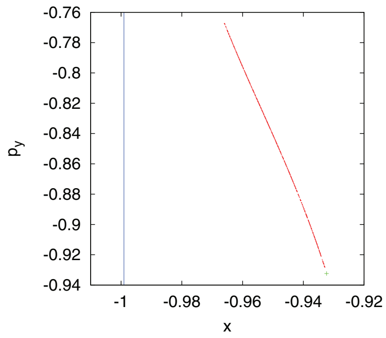

Figure 6. *Numerical plot of $\kappa(x)$, consisting of 15 000 points q_i^0 on Lyapunov orbits (in red). The point L_2 is in green. The blue line $x = -1 + \mu$ gives an indication of the position of the smaller primary along the x coordinate.*

then there exists a smooth function $\kappa : I \to \mathbb{R}$ such that for any $x \in I$ a point $q(x) = (x, 0, 0, \kappa(x))$ lies on an S-symmetric periodic orbit of (2.3). Moreover, $\kappa'(x) \in [\underline{\alpha}, \overline{\alpha}]$ and $q(x) \in U$ for all $x \in I$.

Proof. Existence of a unique point $\kappa(x_0) \in J_0$ for which $g_{x_0}(\kappa(x_0)) = 0$ follows from (3.3), which implies

$$p_y^0 - [Dg_{x_0}(J_0)]^{-1} g_{x_0}(p_y^0) \subset N \subset J_0,$$

combined with interval Newton method (Theorem 2.1).

For (3.4) to hold we need to have $0 \notin dP(U)_{23}$. For $(x, 0, p_y) \in U$ we have $\frac{\partial f}{\partial p_y}(x, p_y) \in dP(U)_{23}$; hence $\frac{\partial f}{\partial p_y}(x, p_y) \neq 0$. This means that we can apply the implicit function theorem to obtain a curve $\kappa(x)$ for which $f(x, \kappa(x)) = 0$. We now need to make sure that the curve κ is defined on the entire interval I. At each point x for which $(x, 0, \kappa(x)) \in U$ is defined, by the implicit function theorem we know that

$$\kappa'(x) = -\frac{\frac{\partial f}{\partial x}(x, \kappa(x))}{\frac{\partial f}{\partial p_y}(x, \kappa(x))} \in \left[-\frac{dP(U)_{21}}{dP(U)_{23}}\right].$$

This, by assumption (3.4), means that we can continue the curve from $\kappa(x^0)$ to the whole interval I (see Figure 5). ∎

To apply Lemma 3.1 we first compute numerically a sequence of points (see Figure 6)

$$q_i^0 = (x_i^0, 0, 0, p_{y,i}^0) \quad \text{for} \quad i = 0, \ldots, 15\,000,$$
$$x_i^0 = \underline{I_x} + \frac{i}{15000}\left(\overline{I_x} - \underline{I_x}\right),$$

where $\underline{I_x}$, $\overline{I_x}$ are defined in (3.1). The q_i^0 are nonrigorously numerically computed points on Lyapunov orbits. We then compute (nonrigorously) a sequence of slopes (see Figure 7)

$$a_i \in \mathbb{R}, \quad i = 0, \ldots, 15\,000,$$

define

$$r = \frac{1}{15\,000}\frac{1}{2}(\overline{I_x} - \underline{I_x}) \approx 10^{-6} \cdot 1.1007716,$$

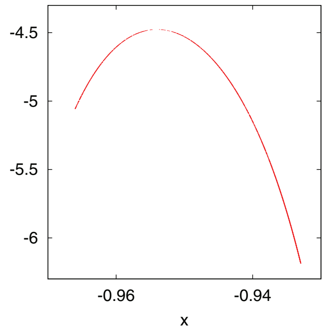

Figure 7. *Numerical plot of $\kappa'(x)$, consisting of 15 000 points a_i.*

$$
\begin{aligned}
I_i &= x_i^0 + [-r, r]\,,\\
J_{0,i} &= p_{y,i}^0 + 10^{-13}\cdot[-1,1],\\
J_{1,i} &= p_{y,i}^0 + 10^{-8}\cdot[-5,5]\,,
\end{aligned}
$$

and consider sets

$$
\begin{aligned}
U_0 &= \{x_i^0\}\times\{0\}\times J_{0,i},\\
U_i &= \left\{(x,0,p_y)|x\in I_i, p_y = a_i\left(x-x_i^0\right)+\iota, \iota\in J_{1,i}\right\}.
\end{aligned}
$$

We apply Lemma 3.1 repeatedly 15 000 times and obtain the following theorem.

Theorem 3.2 (first main result). *Let I_x be the interval from (3.1). Then there exists a curve $q(x) = (x,0,0,\kappa(x))$ of points on Lyapunov orbits with $\kappa : I_x \to \mathbb{R}$, which lies within a $5\cdot 10^{-8}$ distance from the piecewise linear curve joining the 15 000 points q_i^0 on Figure 6.*

The proof of Theorem 3.2 took 5 hours and 43 minutes on a single core 2.53 GHz laptop with 4 GB of RAM.

Remark 3.3. *Let us note that the computation of the Poincaré map and of its derivative cannot be performed analytically. In our application, these are computed using an interval arithmetic based integrator from the CAPD package (for more details, see section 9.3).*

Remark 3.4. *Using the above method it is impossible to continue with the orbits to L_2. At the fixed point one would need to apply alternative methods, such as the method of majorants [21], the Lyapunov theorem by tracing the radius of convergence of the normal form [20], or topological computer assisted tools such as those in [8, 10].*

4. Outline of results for intersections of invariant manifolds. In the remainder of the paper we shall focus our attention on orbits starting from $q(x^*) = (x^*,0,0,\kappa(x^*))$ with $x^*\in I$ for

$$
\begin{aligned}
I = [\underline{I},\overline{I}] &:= x^0 + [-1,1]\cdot 10^{-9},\\
x^0 &= -0.9510055339445208.
\end{aligned}
\tag{4.1}
$$

Such orbits have energy close to the energy of the comet Oterma $h = 1.515$.

In the following, we reserve the notation x^* for the points from the interval I given in (4.1). We also use the notation Λ for a family of Lyapunov orbits, which start from $q(x^*)$ with $x^* \in I$:

$$\Lambda = \{\phi(t, q(x^*)) | t \in \mathbb{R}, q(x^*) = (x^*, 0, 0, \kappa(x^*)), x^* \in I\}. \tag{4.2}$$

For $x^* \in I$, let $L(x^*) \subset \Lambda$ denote the Lyapunov orbit which starts from $q(x^*)$.

Throughout the remainder of the paper we shall prove the following theorem.

Theorem 4.1 (second main result). *Λ is a normally hyperbolic invariant manifold with a boundary. Each orbit $L(x^*) \subset \Lambda$ possesses a two dimensional stable manifold $W^s(L(x^*))$ and a two dimensional unstable manifold $W^u(L(x^*))$. The manifolds $W^s(L(x^*))$ and $W^u(L(x^*))$ intersect, and the intersection, when restricted to the constant energy manifold $M(H(L(x^*)))$, is transversal (see (2.4) for the definition of M).*

Numerical plots of the intersection of manifolds that we shall prove are given in Figure 3.

Theorem 4.1 will be proved with computer assistance. During the proof we shall obtain rigorous bounds on the region and the angle at which the manifolds intersect (see Figure 14).

The size of interval I (4.1) is very small. When translated to the real-life distance in the Jupiter–Sun system, its length is just slightly over one and a half kilometers. This is practically a single point. We need to start with such a small set to obtain our result. Thanks to this we obtain sharp estimates on the intersection of $W^s(L(x^*))$, $W^u(L(x^*))$. To consider a larger set of Lyapunov orbits one would need to iterate the procedure a number of times. This can be done without any difficulty apart from necessary time for computation. The proof of Theorem 4.1 took 46 minutes on a single core 2.53 GHz laptop with 4 GB of RAM. Using clusters one could cover a larger interval I in reasonable time.

5. Hyperbolicity of Lyapunov orbits and foliation by energy.

In this section we show that each orbit $L(x^*) \subset \Lambda$ lies on a different energy level. We also show that each orbit $L(x^*)$ (when considered on its constant energy manifold) is hyperbolic. In other words, we shall show that Λ is a normally hyperbolic manifold with a boundary.

We start with a simple remark.

Remark 5.1. *If for all $x^* \in I$ we have $\frac{d}{dx}H(q(x^*)) \neq 0$, then Lyapunov orbits with different x^* have different energies. Note that the set U and the bound on the derivative of $\kappa'(x^*)$ from Lemma 3.1 can be used to obtain*

$$\frac{d}{dx}H(q(x^*)) \in \left[\frac{\partial H}{\partial x}(U) + \frac{\partial H}{\partial p_y}(U)\kappa'(U)\right].$$

We shall now give a simple lemma which can be used to show that our Lyapunov orbits are hyperbolic.

In what follows in this section, let $P^2 : \Sigma \to \Sigma$ be a second return Poincaré map for $\Sigma = \{y = 0\}$. This means that each point $q(x^*) = (x^*, 0, 0, \kappa(x^*))$, with $x^* \in I$, is a fixed point of P^2. We shall interpret the Poincaré map as a function from $\mathbb{R}^3$ to $\mathbb{R}^3$ with coordinates x, p_x, p_y.

Lemma 5.2. *Let U be the set given by (3.2) in Lemma 3.1. Assume that for any 1×2*

matrix A satisfying

$$A \in \left[\left(-\left(\frac{\partial H}{\partial x}\right)^{-1}\begin{pmatrix} \frac{\partial H}{\partial p_x} & \frac{\partial H}{\partial p_y}\end{pmatrix}\right)(U)\right] \tag{5.1}$$

and any 2×2 matrix B satisfying

$$B \in \left[\left(\begin{pmatrix} dP^2_{21} \\ dP^2_{31}\end{pmatrix} A + \begin{pmatrix} dP^2_{22} & dP^2_{23} \\ dP^2_{32} & dP^2_{33}\end{pmatrix}\right)(U)\right] \tag{5.2}$$

the spectrum of B consists of two real eigenvalues λ_1, λ_2 satisfying $|\lambda_1| > 1 > |\lambda_2|$. Then for any $x^* \in I$ the Lyapunov orbit starting from $q(x^*)$, restricted to the constant energy manifold $M(H(q(x^*)))$, is a hyperbolic orbit.

Proof. Let us fix some $\hat{x} \in I$. For our assumptions to hold, A from (5.1) needs to be properly defined. This means that $\frac{\partial H}{\partial x}(q(\hat{x})) \neq 0$. By the implicit function theorem there exists a function $x(p_x, p_y)$ with $x(0, \kappa(\hat{x})) = \hat{x}$ such that $H(x(p_x, p_y), 0, p_x, p_y) = H(q(\hat{x}))$ and

$$\begin{pmatrix} \frac{\partial x}{\partial p_x} & \frac{\partial x}{\partial p_y}\end{pmatrix}(0, \kappa(\hat{x})) = -\left(\frac{1}{\frac{\partial H}{\partial x}}\begin{pmatrix} \frac{\partial H}{\partial p_x} & \frac{\partial H}{\partial p_y}\end{pmatrix}\right)(0, \kappa(\hat{x})). \tag{5.3}$$

The Lyapunov orbit starting from $q(\hat{x})$ is contained in the constant energy manifold $M(H(q(\hat{x})))$. Let us consider $V = M(H(q(\hat{x}))) \cap \{y = 0\}$ and a Poincaré map $\tilde{P}^2 : V \to V$. In a neighborhood of $q(\hat{x})$ the manifold V can be parameterized by (p_x, p_y). Since

$$\tilde{P}^2(p_x, p_y) = \pi_{(p_x,p_y)} P^2(x(p_x, p_y), p_x, p_y),$$

we have

$$\begin{aligned} &D\tilde{P}^2 (0, \kappa(\hat{x})) \\ &= \left(\left(\pi_{(p_x,p_y)}\frac{\partial P^2}{\partial x}\right)\begin{pmatrix} \frac{\partial x}{\partial p_x} & \frac{\partial x}{\partial p_y}\end{pmatrix} + \begin{pmatrix} dP^2_{22} & dP^2_{23} \\ dP^2_{32} & dP^2_{33}\end{pmatrix}\right)(\hat{x}, 0, \kappa(\hat{x})). \end{aligned} \tag{5.4}$$

By (5.3), (5.4), and our assumption about the spectrum of B of from (5.2), it follows that $(0, \kappa(\hat{x}))$ is a hyperbolic fixed point for the map $\tilde{P}^2$. This means that the Lyapunov orbit starting from $q(\hat{x})$, restricted to the constant energy manifold $M(H(q(\hat{x})))$, is hyperbolic. ∎

Remark 5.3. *Since B from (5.2) is a 2×2 matrix, estimation of its eigenvalues is straightforward. Here we profit from the reduction of dimension made by restricting our attention to a constant energy manifold.*

Since we consider a small part of the family of orbits (4.1), we can obtain a much tighter enclosure of the curve $\kappa(x^*)$ for $x^* \in I$ than from Theorem 3.2. Let

$$\begin{aligned} p^0_y &= -0.836804179646973, \qquad & J_0 &= p^0_y + [-1, 1] \cdot 10^{-13}, \\ a &= -4.506866203376769, & J_1 &= p^0_y + [-1, 1] \cdot 10^{-12}, \end{aligned} \tag{5.5}$$

and

$$U = \left\{(x^*, 0, 0, p_y) | x^* \in I, p_y = a\left(x^* - x^0\right) + \iota, \iota \in J_1\right\}. \tag{5.6}$$

Proposition 5.4. *For $x^* \in I$, with I from* (4.1)*, we have $q(x^*) = (x^*, 0, 0, \kappa(x^*)) \subset U$ and*

$$\kappa'(x^*) \in [-4.506980818, -4.506751634], \tag{5.7}$$

$$\frac{d}{dx} H(q(x^*)) \in [-0.3670937615, -0.3670674516], \tag{5.8}$$

$$H(\underline{I}, 0, 0, a(\underline{I} - x_0) + J_1) \in [-1.514999999635, -1.514999999631],$$
$$H(\overline{I}, 0, 0, a(\overline{I} - x_0) + J_1) \in [-1.515000000369, -1.515000000365].$$

Moreover, the orbits (when considered on their constant energy manifolds) are hyperbolic, and we have the following bounds for the eigenvalues:

$$\begin{aligned} \lambda_1 &\in [1450.24, 1481.68], \\ \lambda_2 &\in 10^{-4} [6.74909, 6.89541]. \end{aligned} \tag{5.9}$$

Proof. The proof was performed with computer assistance. It required no subdivision of U, and the computation took less than two seconds on a single core 2.53 GHz laptop with 4 GB of RAM.

Existence of $q(x^*) \subset U$ was shown using Lemma 3.1. From it also follows the bound (5.7) for $\kappa'(x^*)$. The bound (5.8) follows from Remark 5.1. Hyperbolicity and bounds (5.9) follow from Lemma 5.2. ■

6. Cone conditions and bounds for unstable manifolds of saddle-center fixed points.

In this section we provide a topological tool that can be used for rigorous computer assisted detection of unstable manifolds of saddle-center fixed points. The method is a modification of [25], where, instead of a saddle-center fixed point, a standard hyperbolic fixed point was considered. The contents of this section are a general result. In section 7 we return to the PCR3BP and show how to apply it to prove Theorem 4.1.

Let $F : \mathbb{R}^4 \to \mathbb{R}^4$ be a C^k diffeomorphism with a fixed point $v^* \in \mathbb{R}^4$ and $k \geq 1$. Assume that for eigenvalues $\lambda_1, \lambda_2, \lambda_3, \lambda_4$ from the spectrum of $DF(v^*)$ we have

$$\begin{aligned} |\mathrm{Re}\lambda_1| &> m > 1, \\ |\mathrm{Re}\lambda_i| &< m \quad \text{for } i = 2, 3, 4. \end{aligned} \tag{6.1}$$

Let $W^u(v^*)$ denote the unstable manifold of v^* associated with the eigenvalue λ_1:

$$W^u(v^*) = \left\{ v | \left\| F^{-n}(v) - v^* \right\| < Cm^{-n} \text{ for all } n \in \mathbb{N} \text{ and some } C > 0 \right\}.$$

Let $u = 1$ and $c = 3$. The notation u and c will stand for "unstable" and "central" coordinates of F at v^*. Consider two balls B_u and B_c, of dimensions u and c, respectively, such that $B_u \times B_c$ is centered at v^*. For a point $v \in \mathbb{R}^u \times \mathbb{R}^c$ we shall write $v = (\mathsf{x}, \mathsf{y})$, with $\mathsf{x} \in \mathbb{R}^u$, $\mathsf{y} \in \mathbb{R}^c$. In this notation we shall also write the fixed point as $v^* = (\mathsf{x}^*, \mathsf{y}^*)$.

Remark 6.1. *We do not need to assume that $(\mathsf{x}, 0)$ is the eigenvector associated with λ_1 and that vectors $(0, \mathsf{y})$ span the eigenspace of $\lambda_2, \lambda_3, \lambda_4$. For our method to work it is enough if these vectors are "roughly" aligned with the eigenspaces. This is important for us, since in*

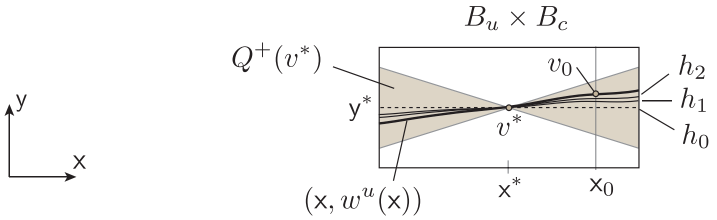

Figure 8. *Construction of the curve $(\mathsf{x}, w^u(\mathsf{x}))$ which lies on the unstable manifold of v^*.*

any computer assisted computation it is usually not possible to compute the eigenvectors with full precision.

Let $\alpha \in \mathbb{R}$, $\alpha > 0$, and consider a function $Q : \mathbb{R}^u \times \mathbb{R}^c \to \mathbb{R}$:

$$Q(\mathsf{x}, \mathsf{y}) = \alpha \mathsf{x}^2 - \|\mathsf{y}\|^2 .$$

For $v_0 \in \mathbb{R}^u \times \mathbb{R}^c$ we shall use the notation $Q^+(v_0)$ for a cone

$$Q^+(v_0) = \{v | Q(v - v_0) \geq 0\} .$$

Let us assume that α is chosen sufficiently small so that $Q^+(v^*) \cap B_u \times B_c$ does not intersect with $B_u \times \partial B_c$ (see Figure 8).

Definition 6.2. *We shall say that $h : B_u \to B_u \times B_c$ is a* horizontal disk in $B_u \times B_c$ for cones given by Q *if $h(\mathsf{x}^*) = v^*$, $\pi_{\mathsf{x}} h(\mathsf{x}) = \mathsf{x}$, and for any $\mathsf{x}_1 \neq \mathsf{x}_2$ we have $Q(h(\mathsf{x}_1) - h(\mathsf{x}_2)) > 0$.*

Lemma 6.3. *Assume that, for any $v_1, v_2 \in Q^+(v^*)$ such that $Q(v_1 - v_2) \geq 0$, we have*

$$Q(F(v_1) - F(v_2)) > 0. \tag{6.2}$$

Let m be the constant from (6.1). If for any $v \in B_u \times B_c$, $v \neq v^*$, and $Q(v - v^*) \geq 0$ the condition

$$\|F(v) - v^*\| > m \|v - v^*\| \tag{6.3}$$

holds, then $W^u(v^*) \subset Q^+(v^*)$. Moreover, there exists a function $w^u : B_u \to B_c$ such that $(id, w^u)(B_u) = W^u(v^*) \cap B_u \times B_c$, and for any $\mathsf{x}_1, \mathsf{x}_2 \in B_u$, $\mathsf{x}_1 \neq \mathsf{x}_2$,

$$Q((\mathsf{x}_1, w^u(\mathsf{x}_1)) - (\mathsf{x}_2, w^u(\mathsf{x}_2))) > 0 \tag{6.4}$$

and

$$\left\|(w^u)'(\mathsf{x})\right\| \leq \sqrt{\alpha} \quad \textit{for all } \mathsf{x} \in B_u. \tag{6.5}$$

Proof. We shall first show that for any $\mathsf{x}_0 \in B_u \backslash \{\mathsf{x}^*\}$ there exists a point $v_0 = (\mathsf{x}_0, w^u(\mathsf{x}_0)) \in Q^+(v^*)$ such that $v_0 \in W^u(v^*)$. Let $h_0(\mathsf{x}) = (\mathsf{x}, \mathsf{y}^*)$ be a horizontal disk (see Figure 8). Observe that $F(h_0(\mathsf{x}^*)) = F(\mathsf{x}^*, \mathsf{y}^*) = v^*$. By assumptions (6.2) and (6.3) the curve $F(h_0(\mathsf{x}))$ is contained in $Q^+(v^*)$ and $F(h_0(\partial B_u)) \cap B_u \times B_c = \emptyset$. Moreover, since by the definition of h_0 we see that for any $\mathsf{x}_1, \mathsf{x}_2 \in B_u$, $\mathsf{x}_1 \neq \mathsf{x}_2$,

$$Q(h_0(\mathsf{x}_1) - h_0(\mathsf{x}_2)) > 0,$$

by assumption (6.2) we obtain

$$Q(F(h_0(\mathsf{x}_1)) - F(h_0(\mathsf{x}_2))) > 0,$$

which means that $\{F(h_0(\mathsf{x}))|\mathsf{x} \in B_u\} \cap B_u \times B_c$ is a graph of a horizontal disk. Let us denote this disk by h_1 and observe that $h_1(\mathsf{x}^*) = v^*$. In other words, let h_1 be the graph transform of the disk h_0.

Taking $F(h_1(\mathsf{x}))$ and applying an identical argument, we observe that

$$\{F(h_1(\mathsf{x}))|\mathsf{x} \in B_u\} \cap B_u \times B_c$$

is a graph of a horizontal disk h_2. Repeating this procedure, we can construct a sequence of horizontal disks $h_0, h_1, h_2, \dots$. For a fixed x_0, due to the compactness of closure of B_c, there exists a subsequence $h_{k_i}(\mathsf{x}_0)$ convergent to some point $v_0 \in B_u \times \mathrm{cl}B_c$. For any $i, n \in \mathbb{N}$ with $k_i > n$ the point $F^{-n}(h_{k_i}(\mathsf{x}_0))$ lies on the graph of $h_{k_i - n}$ and hence is also in $Q^+(v^*)$. This means that for any $n \in \mathbb{N}$

$$F^{-n}(v_0) = \lim_{i\to\infty} F^{-n}(h_{k_i}(\mathsf{x}_0)) \in Q^+(v^*).$$

By assumption (6.3) we have

$$\left\|F^{-n}(v_0) - v^*\right\| < \frac{1}{m^n} \left\|v_0 - v^*\right\|,$$

which means that $v_0 \in W^u(v^*)$. By construction $\pi_{\mathsf{x}} v_0 = \mathsf{x}_0$; hence we can define $w^u(\mathsf{x}_0) := \pi_{\mathsf{y}} v_0$.

By the stable/unstable manifold theorem (see, for instance, [7]), there exists a small interval $I_\varepsilon = (\mathsf{x}^* - \varepsilon, \mathsf{x}^* + \varepsilon)$ in which $\{(\mathsf{x}, w^u(\mathsf{x}))|\mathsf{x} \in I_\varepsilon\}$ is a C^k curve which gives a full description of $W^u(v^*)$. Since $(\mathsf{x}, w^u(\mathsf{x})) \subset Q^+(v^*)$ we have $(1, (w^u)'(\mathsf{x}^*)) \in Q^+(0)$. Since for sufficiently small ε the vector $(1, (w^u)'(\mathsf{x}))$ is arbitrarily close to $(1, (w^u)'(\mathsf{x}^*))$, for $\mathsf{x}_1, \mathsf{x}_2 \in I_\varepsilon$

$$Q\left((\mathsf{x}_1, w^u(\mathsf{x}_1)) - (\mathsf{x}_2, w^u(\mathsf{x}_2))\right) > 0. \tag{6.6}$$

Iterating the curve $(\mathsf{x}, w^u(\mathsf{x}))$ through F, by (6.2) and (6.3) we obtain our function $w^u : B_u \to B_c$. Note that by our construction for any $\mathsf{x}_1, \mathsf{x}_2 \in B_u$ inequality (6.6) holds. This implies that for any $\mathsf{x}_1, \mathsf{x}_2 \in B_u$

$$\frac{\|w^u(\mathsf{x}_1) - w^u(\mathsf{x}_2)\|^2}{|\mathsf{x}_1 - \mathsf{x}_2|^2} < \alpha,$$

which in turn gives (6.5). ■

Remark 6.4. *Lemma 6.3 can easily be generalized to higher dimensions of $W^u(v^*)$ and to $F : \mathbb{R}^l \to \mathbb{R}^l$ with $l > 4$. The proof would be identical, taking $Q(\mathsf{x}, \mathsf{y}) = \alpha\|\mathsf{x}\|^2 - \|\mathsf{y}\|^2$. Here we have set up our discussion so that $W^u(v^*)$ is one dimensional and $l = 4$ simply because this is what we shall need for our application to the PCR3BP.*

Remark 6.5. *By taking the inverse map, Lemma 6.3 can be used to prove existence of stable manifolds.*

To verify assumptions (6.2) and (6.3) in practice, it is best to make use of an interval matrix $\mathbf{A} = [DF(Q^+(v^*))]$. Then for any $v_1, v_2 \in Q^+(v^*)$ we have

$$F(v_1) - F(v_2) = \int_0^1 DF\left(v_2 + t\left(v_1 - v_2\right)\right) dt \cdot \left(v_1 - v_2\right) \in \mathbf{A}\left(v_1 - v_2\right). \tag{6.7}$$

This means that

$$F(v) - v^* \subset \mathbf{A}\left(v - v^*\right). \tag{6.8}$$

To verify (6.3) using (6.8) we can apply Lemma 9.1 from the appendix.

Let us now turn to the verification of (6.2). Let C_Q be a diagonal matrix such that $v^T C_Q v = Q(v)$. Equation (6.7) gives an estimate

$$Q\left(F(v_1) - F(v_2)\right) \subset \left(v_1 - v_2\right)^T \mathbf{A}^T C_Q \mathbf{A}\left(v_1 - v_2\right). \tag{6.9}$$

To verify (6.2) using (6.9) we can apply Lemma 9.2 from the appendix.

We see that the assumptions of Lemma 6.3 follow from bounds on the derivative of the map.

Remark 6.6. *Let us note that to apply the lemma we do not need hyperbolicity of the fixed point. The fixed point can, in particular, be a saddle center. We can also apply the lemma for a set of fixed points in $B_u \times B_c$, provided that we know that such a set exists, and provided that for each fixed point v^* from the set, its unstable fiber will lie in $Q^+(v^*)$. Existence of unstable fibers for the set of fixed points can follow from the same interval matrix estimate on the derivative of the map on $B_u \times B_c$.*

7. Rigorous bounds for invariant manifolds associated with Lyapunov orbits.

In this section we give a proof of Theorem 4.1. In sections 7.1 and 7.2 we shall show how to apply the method from section 6 to detect fibers of unstable manifolds of Lyapunov orbits. In section 7.3 we shall show how to prove that the manifolds intersect. Using these results, in section 7.4 we give a computer assisted proof Theorem 4.1.

7.1. Parameterization method.

The method from section 6 requires a good change of coordinates which "straightens out" the unstable manifold. We shall obtain such a change of coordinates using a parameterization method. In this subsection we give an outline of this procedure.

In this section we shall fix some $x^* \in I$ (see (4.1) for I) and show how to find an unstable fiber of a point

$$q_0 = q(x^*) = (x^*, 0, 0, \kappa(x^*)) \in L(x^*).$$

We shall use the notation $\tau = \tau(q_0)$ for the return time along the trajectory. The point q_0 is a saddle-center fixed point for a τ-time map $\Phi_\tau : \mathbb{R}^4 \to \mathbb{R}^4$.

Let C denote a matrix which brings $D\Phi_\tau(q_0)$ to real Jordan form. By $\tilde{\Phi}_\tau : \mathbb{R}^4 \to \mathbb{R}^4$ we shall denote the time τ map in the linearized local coordinates

$$\tilde{\Phi}_\tau(v) := C^{-1}\left(\Phi_\tau\left(q_0 + Cv\right) - q_0\right).$$

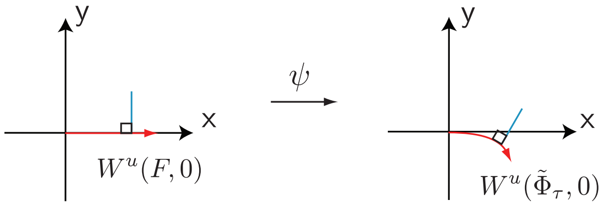

Figure 9. *The nonlinear change of coordinates* ψ.

We know that $D\tilde{\Phi}_\tau(0)$ has a single eigenvalue λ with real part greater than one. We use $W^u(\tilde{\Phi}_\tau,0)$ to denote the unstable manifold of $\tilde{\Phi}_\tau$ at zero associated with λ. If we can find a function

$$K = (K_0, K_1, K_2, K_3) : \mathbb{R} \to \mathbb{R}^4,$$

which for all x in an interval $I_0 = [\underline{\mathsf{x}}, \overline{\mathsf{x}}]$, $\underline{\mathsf{x}} < 0 < \overline{\mathsf{x}}$, is a solution of a cohomology equation

$$\tilde{\Phi}_\tau(K(\mathsf{x})) = K(\lambda \mathsf{x}), \tag{7.1}$$

then $K(\mathsf{x}) \subset W^u(\tilde{\Phi}_\tau,0)$ for $\mathsf{x} \in I_0$.

Once K is established we can consider a nonlinear change of coordinates

$$\psi = (\psi_0, \psi_1, \psi_2, \psi_3) : \mathbb{R}^4 \to \mathbb{R}^4$$

defined as

$$\begin{aligned} \psi_0(\mathsf{x}, \mathsf{y}_1, \mathsf{y}_2, \mathsf{y}_3) &= K_0(\mathsf{x}) - \left(\mathsf{y}_1 K_1'(\mathsf{x}) + \mathsf{y}_2 K_2'(\mathsf{x}) + \mathsf{y}_3 K_3'(\mathsf{x})\right), \\ \psi_i(\mathsf{x}, \mathsf{y}_1, \mathsf{y}_2, \mathsf{y}_3) &= K_i(\mathsf{x}) + \mathsf{y}_i K_0'(\mathsf{x}) \quad \text{for } i = 1,2,3. \end{aligned} \tag{7.2}$$

Note that $\psi(\mathsf{x},0) = K(\mathsf{x})$ gives points on the unstable manifold of the fixed point for the map $\tilde{\Phi}_\tau$. The intuitive idea behind (7.2) is to arrange the coordinates so that $\psi(\mathsf{x}, \mathsf{y}_1, \mathsf{y}_2, \mathsf{y}_3) - K(\mathsf{x})$ is orthogonal to $K'(\mathsf{x})$ (see Figure 9).

Let us define a local map

$$F = \psi^{-1} \circ \tilde{\Phi}_\tau \circ \psi.$$

Such map will play the role of F from section 6. Observe that

$$\{C\psi(K(\mathsf{x})) + q_0 | \mathsf{x} \in I_0\} \subset C\psi(W^u(F,0)) + q_0 = W^u(\Phi_\tau, q_0) \subset W^u(L(x_0)).$$

7.2. Bounds for unstable fibers through parameterization and cone conditions. The map ψ (7.2) gives us a change of coordinates which locally "straightens out" the unstable manifold. The problem with applying the procedure from section 7.1 in practice lies in the fact that usually finding an analytic formula for K satisfying (7.1) is impossible. The best that can be done is to find a K which is a polynomial approximation of a solution of (7.1). This can be done by expanding $\tilde{\Phi}_\tau$ into a Taylor series and inductively comparing the coefficients in (7.1) (for a detailed description of this method we refer the reader to [7]; see, in particular, section 4 and Theorem 4.1). If we find such an approximate solution of (7.1), then the set $\{(\mathsf{x},0) | \mathsf{x} \in I_0\}$ is no longer the unstable manifold for F (defined by (7.3)) but its approximation.

Even though our description of the unstable fiber is then not entirely accurate, we can apply the method from section 6 to obtain a rigorous enclosure of $W^u(F,0)$. This enclosure can then be transported to the original coordinates.

In this section we shall assume that q_0 is an arbitrary point close to $q(x^*) = (x^*, 0, 0, \kappa(x^*))$ for $x^* \in I$, for I from (4.1). We also assume that C is some given matrix, that $K : \mathbb{R} \to \mathbb{R}^4$ is some given polynomial, and that ψ is defined by (7.2).

Remark 7.1. *Let us stress that the point q_0 is a numerical approximation of $q(x^*)$, and the matrix C will be a (nonrigorous) numerically obtained estimate for the change into Jordan form of the map Φ_τ. We do not assume that this change is rigorously computed. This is practically impossible due to the fact that we do not have an analytic formula for $D\Phi_\tau(q_0)$. For us the matrix C is simply some approximation of the matrix which takes $D\Phi_\tau(q_0)$ into Jordan form. Let us note that it is not difficult to find an interval matrix $\mathbf{C}^{-1}$ such that the inverse matrix of our C is contained in $\mathbf{C}^{-1}$.*

Remark 7.2. *In our setting the polynomial K is an approximation of the solution of (7.1). In practice we cannot obtain a fully rigorous solution of (7.1). It is important to emphasize that we also do not have an inverse of ψ. It is also not simple to find good rigorous estimates for the function ψ^{-1} due to the fact that K is a vector of polynomials of degree 4. We shall therefore set up all our subsequent computations so that we will never need to use the inverse function of ψ.*

For $x^* \in I$, let $\tau(x^*)$ be the period of an orbit $L(x^*) \subset \Lambda$. We define a map

$$F = \psi^{-1} \circ \tilde{\Phi}_{\tau(x^*)} \circ \psi. \tag{7.3}$$

Note that for each $x^* \in I$ we have a different map F. We omit this in our notation for simplicity, and also because the methods described below for obtaining rigorous bounds for F and its derivative shall work for all $x^* \in I$.

Recall that in Proposition 5.4 we have shown that for I defined in (4.1) and for U defined in (5.6)

$$\{q(x^*) = (x^*, 0, 0, \kappa(x^*)) : x^* \in I\} \subset U.$$

We shall first be interested in computing rigorous bounds for $F(U)$. It turns out that (7.3) is impossible to apply since we do not have a formula for ψ^{-1}. Even if we did, direct application of (7.3) in interval arithmetic would provide very bad estimates due to strong hyperbolicity of the map. We use a more subtle method.

We shall first need the following notation. Let $\boldsymbol{T}$ denote an interval such that $\tau(x^*) \in \boldsymbol{T}$ for all $x^* \in I$. Let $\tilde{\lambda} \in \mathbb{R}$ be some number close to an unstable eigenvalue of $D\Phi_{\tau(x^*)}(q(x^*))$ for some $x^* \in I$. We shall slightly abuse notation and also consider $\tilde{\lambda} : \mathbb{R}^4 \to \mathbb{R}^4$ as a function defined on $v = (\mathsf{x}, \mathsf{y}) \in \mathbb{R} \times \mathbb{R}^3$ as

$$\tilde{\lambda}(\mathsf{x}, \mathsf{y}) := (\tilde{\lambda}\mathsf{x}, \mathsf{y}).$$

The following lemma allows us to obtain rigorous bounds on preimages of F from (7.3).

Lemma 7.3. *Let $U_1 \subset \mathbb{R}^4$ be a given set. Let $G : \mathbb{R} \times \mathbb{R}^4 \times \mathbb{R}^4 \to \mathbb{R}^4$ be defined as*

$$G(\tau, v_1, v_2) = \Phi_\tau(C\psi(v_1) + q_0) - \left(C\psi(\tilde{\lambda}(v_2)) + q_0\right). \tag{7.4}$$

Let $U_2 \subset \mathbb{R}^4$ *be a set and* $\mathbf{A}(U_2)$ *be an interval matrix defined as*

$$\mathbf{A}(U_2) = -\left[CD\psi\left(\tilde{\lambda}(U_2)\right)D\tilde{\lambda}\right].$$

If for some $v_0 \in U_2$

$$N(\mathbf{T}, v_0, U_1, U_2) := v_0 - [\mathbf{A}(U_2)]^{-1}[G(\mathbf{T}, U_1, v_0)] \subset U_2, \tag{7.5}$$

then

$$F(U_1) \subset \tilde{\lambda}(U_2). \tag{7.6}$$

Proof. The proof is given in the appendix in section 9.2. See also Remark 9.4 for comments on the practical application of the lemma. ∎

Remark 7.4. *The choice of the function* G *is motivated by the following diagram:*

$$\begin{array}{ccc}
\mathbb{R}^4 & \xrightarrow{\Phi_\tau} & \mathbb{R}^4 \\
\uparrow C + q_0 & & \uparrow C + q_0 \\
\mathbb{R}^4 & \xrightarrow{\tilde{\Phi}_\tau} & \mathbb{R}^4 \\
\uparrow \psi & & \uparrow \psi \\
\mathbb{R}^4 & \left(\xrightarrow{\tilde{\lambda}}\right) & \mathbb{R}^4
\end{array}$$

The diagram is not fully commutative; hence we have the parentheses for $\tilde{\lambda}$. *Intuitively, for* $v = (\mathsf{x}, 0) \in \mathbb{R} \times \mathbb{R}^3$ *the diagram should "almost commute." Even though this statement is nowhere close to rigorous, it might make the method and proof of Lemma 7.3 more intuitive.*

We now turn to the computation of rigorous bounds for the derivatives of (7.3). For any (x, y) contained in a set $B \subset \mathbb{R}^4$ we have the following estimates:

$$\begin{aligned}
DF(\mathsf{x}, \mathsf{y}) &= (D\psi(F(\mathsf{x}, \mathsf{y})))^{-1} C^{-1} D\Phi_{\tau(x^*)}(C\psi(\mathsf{x}, \mathsf{y}) + q_0) CD\psi(\mathsf{x}, \mathsf{y}) \\
&\subset \left[(D\psi(F(B)))^{-1}\right] \cdot \left[C^{-1}\right] \cdot [D\Phi_{\mathbf{T}}(C\psi(B) + q_0)] \cdot C \cdot [D\psi(B)] \\
&=: [DF(B)].
\end{aligned} \tag{7.7}$$

Note that to compute $[DF(B)]$ from (7.7) we do not need to use ψ^{-1}.

Remark 7.5. *Using Lemma 7.3 and (7.7), we can in practice compute rigorous bounds for* $[F(B)]$ *and* $[DF(B)]$. *We perform such computations in section 7.4.1 with the use of the CAPD library. The library allows for computation of rigorous estimates for* $\Phi_{\mathbf{T}}$ *and its derivative and for rigorous-enclosure operations on maps and interval matrices.*

Proposition 5.4 gives a bound on a set U (5.6) which contains all fixed points $q(x^*)$, with $x^* \in I$, of the map $\Phi_{\tau(x^*)}$. This set can be transported to local coordinates (x, y). Let $B_0 \subset \mathbb{R}^4$ be a set such that

$$\{\psi^{-1}(C^{-1}(q(x^*) - q_0))\} | x^* \in I\} \subset B_0.$$

Such set can easily be computed using, for example, technical Lemma 9.5 from the appendix.

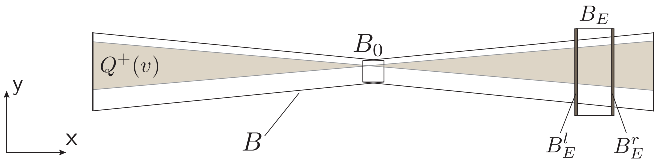

Figure 10. *Local bound on the unstable manifold. Each fixed point $\psi^{-1}(C^{-1}(q(x^*) - q_0))$ for $x^* \in I$ lies in B_0, and its unstable manifold is contained in $B = \bigcup_{v \in B_0} Q^+(v)$.*

Taking a four dimensional set (see Figure 10)

$$B = \bigcup_{v \in B_0} Q^+(v) \subset \mathbb{R}^4$$

and using (7.7) and Lemmas 9.1 and 9.2 to verify the assumptions of Lemma 6.3, we can obtain a bound for the unstable fibers of all $q(x^*)$ for $x^* \in I$. The obtained bound is computed in local coordinates (x, y) but can easily be transported back to the original coordinates (x, y, p_x, p_y) of the system. Detailed results of such a computation will be presented in section 7.4.1.

Remark 7.6. *Let us emphasize that to apply the method it is enough to use a single point q_0, single matrix C, and single nonlinear change ψ. It is not necessary to use different changes to local coordinates for different $x^* \in I$.*

Remark 7.7. *Let us note that from the fact that $W^s(L(x^*))$ is S-symmetric to $W^u(L(x^*))$, without any effort we also obtain mirror bounds for fibers of $W^s(L(x^*))$.*

7.3. Transversal intersections of manifolds. In this section we discuss how the bounds for fibers of $q(x^*)$ discussed in section 7.2 can be used to prove transversal intersections of manifolds $W^u(L(x^*))$ and $W^s(L(x^*))$ for $L(x^*) \subset \Lambda$ (see (4.2) for definition of Λ).

Let $\mathsf{x}^l, \mathsf{x}^r \in \mathbb{R}$ be such that $\mathsf{x}^l < \mathsf{x}^r$ and $\pi_{\mathsf{x}} B_0 < \mathsf{x}^l, \mathsf{x}^r$. Let $B_c \subset \mathbb{R}^3$ be such that $\pi_{\mathsf{y}} B \subset B_c$. Let B_E, B_E^l, B_E^r be defined as (see Figure 10)

$$\begin{aligned} B_E &= [\mathsf{x}^l, \mathsf{x}^r] \times B_c, \\ B_E^l &= \{\mathsf{x}^l\} \times B_c, \\ B_E^r &= \{\mathsf{x}^r\} \times B_c, \end{aligned}$$

and let

$$\begin{aligned} V^+ &= \{(\mathsf{x}, \mathsf{y}_1, \mathsf{y}_2, \mathsf{y}_3) \in \mathbb{R}^4 | \mathsf{x} = 1, \mathsf{y}_i \in [-\sqrt{\alpha}, \sqrt{\alpha}] \text{ for } i = 1, 2, 3\}, \\ V^- &= \{(\mathsf{x}, \mathsf{y}_1, \mathsf{y}_2, \mathsf{y}_3) \in \mathbb{R}^4 | \mathsf{x} = -1, \mathsf{y}_i \in [-\sqrt{\alpha}, \sqrt{\alpha}] \text{ for } i = 1, 2, 3\}, \\ V &= \{\gamma v | v \in V^+, \gamma \geq 0\} \cup \{\gamma v | v \in V^-, \gamma \geq 0\}. \end{aligned}$$

Note that

$$Q^+(0) \subset V.$$

Consider a section

$$\Sigma = \{y = 0\} \cap \{x > 0\} \cap \{p_x^2 < 2\,(H(L(x)) + \Omega(x, y))\}.$$

This shall be a section where we detect the intersection of $W^u(L(x^*))$ and $W^s(L(x^*))$ (see Figures 2 and 3). Let ϕ be the flow of (2.3), and define

$$\tau^u(q) = \inf\{t > 0 : \phi(t,q) \in \Sigma\},$$
$$\mathcal{G} : B_E \to \Sigma,$$
$$\mathcal{G}(\mathsf{x},\mathsf{y}) = \phi(\tau^u(C\psi(\mathsf{x},\mathsf{y}) + q^0), C\psi(\mathsf{x},\mathsf{y}) + q^0).$$

Lemma 7.8. *Assume that for F defined in (7.3), the assumptions of Lemma 6.3 hold. If also*

$$\pi_{p_x}\mathcal{G}(B_E^l) < 0, \qquad \pi_{p_x}\mathcal{G}(B_E^r) > 0, \tag{7.8}$$

then for any $x^* \in I$ (with I defined in (4.1)) the manifolds $W^u(L(x^*))$ and $W^s(L(x^*))$ intersect.

Moreover, if for any $v^+ \in V^+$ and $v^- \in V^-$

$$\begin{aligned} \pi_x [D\mathcal{G}(B_E)]\, v^+ &> 0, \qquad & \pi_{p_x} [D\mathcal{G}(B_E)]\, v^+ &> 0,\\ \pi_x [D\mathcal{G}(B_E)]\, v^- &< 0, \qquad & \pi_{p_x} [D\mathcal{G}(B_E)]\, v^- &< 0, \end{aligned} \tag{7.9}$$

then for each fixed $x^* \in I$ the intersection is transversal on the constant energy manifold $M(H(L(x^*)))$ (see (2.4) for the definition of M).

Remark 7.9. *Computer assisted verification of the assumptions of Lemma 6.3 can be performed for the whole family of maps, defined through (7.3), for all $x^* \in I$ at the same time. To do so we need to conduct our interval computations taking $\tilde{\Phi}_{\boldsymbol{\tau}}$ with an interval $\boldsymbol{\tau} = [\tau(I)]$, which encloses all $\tau(x^*)$ for $x^* \in I$. We can thus use the same point q_0, C, and ψ for all $x^* \in I$.*

Proof of Lemma 7.8. Let us fix an $x^* \in I$. First let us observe that because energy (2.2) is preserved, the manifold $M(L(x^*)) \cap \Sigma$ can be parameterized by x, p_x since

$$p_y = p_y(x, p_x) = \sqrt{2(H(L(x)) + \Omega(x,y)) - p_x^2} + x \tag{7.10}$$

is well defined.

By Lemma 6.3 we know that in local coordinates x,y the unstable fiber of $q(x^*)$ is a horizontal disk in B. This disk is a graph of a function $w^u_{x^*} : B_u \to B_c$, and for any $\mathsf{x}_1, \mathsf{x}_2 \in B_u$ such that $\mathsf{x}_1 \neq \mathsf{x}_2$,

$$(\mathsf{x}_1, w^u_{x^*}(\mathsf{x}_1)) - (\mathsf{x}_2, w^u_{x^*}(\mathsf{x}_2)) \in Q^+(0) \subset V.$$

The disk also passes through the set B_E (see Figure 10).

In the statement of our lemma we implicitly assume that $\mathcal{G}(\mathsf{x},\mathsf{y})$ is well defined for $(\mathsf{x},\mathsf{y}) \in B_E$. This means that

$$W^u(L(x^*)) \cap \Sigma \cap \mathcal{G}(B_E) = \{\mathcal{G}(\mathsf{x}, w^u_{x^*}(\mathsf{x}))\, | \mathsf{x} \in [\mathsf{x}^l, \mathsf{x}^r]\}. \tag{7.11}$$

Let us introduce the notation

$$w^u_{\Sigma,x^*} : [\mathsf{x}^l, \mathsf{x}^r] \to \mathbb{R}^2,$$
$$w^u_{\Sigma,x^*}(\mathsf{x}) = \pi_{x,p_x}\mathcal{G}(\mathsf{x}, w^u_{x^*}(\mathsf{x}))\,.$$

By (7.10) and (7.11) the curve $w^u_{\Sigma,x^*}(\mathsf{x})$ parameterizes a fragment of the intersection of the manifold $W^u(L(x^*))$ with Σ. By assumption (7.8)

$$\pi_{p_x} w^u_{\Sigma,x^*}(\mathsf{x}^l) = \pi_{p_x}\mathcal{G}(\mathsf{x}^l, w^u_{\Sigma,x^*}(\mathsf{x}^l)) \in \pi_{p_x}\mathcal{G}(\{\mathsf{x}^l\}\times B_c) = \pi_{p_x}\mathcal{G}(B^l_E) < 0,$$
$$\pi_{p_x} w^u_{\Sigma,x^*}(\mathsf{x}^r) = \pi_{p_x}\mathcal{G}(\mathsf{x}^r, w^u_{x^*}(\mathsf{x}^r)) \in \pi_{p_x}\mathcal{G}(\{\mathsf{x}^r\}\times B_c) = \pi_{p_x}\mathcal{G}(B^r_E) > 0;$$

hence we have an $\mathsf{x}^m \in (\mathsf{x}^l, \mathsf{x}^r)$ such that

$$\pi_{p_x} w^u_{\Sigma,x^*}(\mathsf{x}^m) = 0.$$

The stable manifold $W^s(L(x))$ is S-symmetric to $W^u(L(x^*))$. This means that a fragment of the intersection of $W^s(L(x^*))$ with Σ is parameterized by

$$w^s_{\Sigma,x^*} : [\mathsf{x}^l, \mathsf{x}^r] \to \mathbb{R}^2,$$
$$w^s_{\Sigma,x^*}(\mathsf{x}) = \left(\pi_x w^u_{\Sigma,x^*}(\mathsf{x}), -\pi_{p_x} w^u_{\Sigma,x^*}(\mathsf{x})\right). \tag{7.12}$$

Since $w^u_{\Sigma,x^*}(\mathsf{x}^m) = w^s_{\Sigma,x^*}(\mathsf{x}^m)$, manifolds $W^u(L(x^*))$ and $W^s(L(x^*))$ intersect at

$$q^* = \mathcal{G}(\mathsf{x}^m, w^u_{x^*}(\mathsf{x}^m)).$$

Now we turn to proving transversality of the intersection at q^*. By (7.10), around q^* the manifold $M(H(L(x^*)))$ is parameterized by x, y, p_x. Therefore, in the proof of transversality we restrict our attention to these coordinates. Since $\mathcal{G}$ is well defined, $W^u(L(x^*))$ must transversally cross $\{y = 0\}$. By symmetry so does $W^s(L(x^*))$. We therefore need only prove that $w^u_{\Sigma,x^*}(\mathsf{x})$ and $w^s_{\Sigma,x^*}(\mathsf{x})$ intersect transversally in $\mathbb{R}^2$.

Let $\mathsf{x}^+ \in (\mathsf{x}^m, \mathsf{x}^r]$, $\gamma = 1/(\mathsf{x}^+ - \mathsf{x}^m)$, and

$$v = \gamma\left((\mathsf{x}^+, w^u_{x^*}(\mathsf{x}^+)) - (\mathsf{x}^m, w^u_{x^*}(\mathsf{x}^m))\right) \in V^+.$$

By the mean value theorem

$$w^u_{\Sigma,x^*}(\mathsf{x}^+) - w^u_{\Sigma,x^*}(\mathsf{x}^m) \in \pi_{x,p_x}\frac{1}{\gamma}[D\mathcal{G}(B_E)]\,v.$$

By (7.9) this implies that

$$\pi_x(w^u_{\Sigma,x^*}(\mathsf{x}^+) - w^u_{\Sigma,x^*}(\mathsf{x}^m)) > 0, \qquad \pi_{p_x}(w^u_{\Sigma,x^*}(\mathsf{x}^+) - w^u_{\Sigma,x^*}(\mathsf{x}^m)) > 0. \tag{7.13}$$

By mirror arguments, for $\mathsf{x}^- \in [\mathsf{x}^l, \mathsf{x}^m)$,

$$\pi_x(w^u_{\Sigma,x^*}(\mathsf{x}^-) - w^u_{\Sigma,x^*}(\mathsf{x}^m)) < 0, \qquad \pi_{p_x}(w^u_{\Sigma,x^*}(\mathsf{x}^-) - w^u_{\Sigma,x^*}(\mathsf{x}^m)) < 0. \tag{7.14}$$

From (7.13), (7.14), and (7.12) we see that $w^u_{\Sigma,x^*}(\mathsf{x})$ and $w^s_{\Sigma,x^*}(\mathsf{x})$ intersect transversally at $w^u_{\Sigma,x^*}(\mathsf{x}^m) = w^s_{\Sigma,x^*}(\mathsf{x}^m)$, which concludes our proof. ■

Remark 7.10. *From the proof of Lemma 7.8 it follows that we have the following estimate on the slope of the curves $w^u_{\Sigma,x^*}(\mathsf{x})$:*

$$\mathbf{a} = \left[\frac{\pi_{p_x} D\mathcal{G}(B_E)V^+}{\pi_x D\mathcal{G}(B_E)V^+}\right] \cup \left[\frac{\pi_{p_x} D\mathcal{G}(B_E)V^-}{\pi_x D\mathcal{G}(B_E)V^-}\right].$$

By S-symmetry of $W^u(L(x^*))$ and $W^s(L(x^*))$ the slope of $w^s_{\Sigma,x^*}(\mathsf{x})$ is in $-\mathbf{a}$.

Once we verify (7.8), then by checking that $\mathbf{a} > 0$ we know that assumption (7.9) needs to hold.

7.4. Proof of Theorem 4.1. In this section we write the computer assisted rigorous bounds, which we obtain using the method from sections 7.2 and 7.3. As a result, we obtain rigorous bounds for the position of fibers of $W^u(L(x^*))$ and for the transversal intersection of $W^u(L(x^*))$ with $W^s(L(x^*))$. By this we obtain the proof of Theorem 4.1.

7.4.1. Bounds for unstable fibers. We start by writing our changes of coordinates needed for application of Lemma 7.3 to the map (7.3) from section 7.2.

We first choose the point $q_0 = (x^0, 0, 0, p_y^0)$ with x^0, p_y^0 given in (4.1) and (5.5), respectively, i.e.,

$$x^0 = -0.9510055339445208,$$
$$p_y^0 = -0.8368041796469730.$$

We choose a matrix C as

$$C = \begin{pmatrix} 0.197841 & -0.197841 & 0 & 0.221884 \\ -0.221884 & -0.221884 & 0.773671 & 0 \\ 1 & 1 & -1 & 0 \\ -0.255717 & 0.255717 & 0 & -1 \end{pmatrix}.$$

We then choose four polynomials,

$$K_0(\mathsf{x}) = 0.1\mathsf{x} - 0.0621591\mathsf{x}^2 + 0.0375888\mathsf{x}^3 - 0.0200645\mathsf{x}^4,$$
$$K_1(\mathsf{x}) = 0.000533561\mathsf{x}^2 - 0.00723085\mathsf{x}^3 + 0.00827176\mathsf{x}^4,$$
$$K_2(\mathsf{x}) = -0.0151949\mathsf{x}^2 + 0.009304476\mathsf{x}^3 - 0.00427633\mathsf{x}^4,$$
$$K_3(\mathsf{x}) = 0.0269670\mathsf{x}^2 - 0.0275820\mathsf{x}^3 + 0.0203022\mathsf{x}^4,$$

which define the nonlinear change of coordinates ψ (see (7.2)). All of the above choices are dictated by (nonrigorous) numerical investigation. The above choices ensure that $C\psi(\mathsf{x}, 0)+q_0$ gives a sufficiently accurate approximation of the position of the unstable fibers of $q(x^*)$ for $x^* \in I$ for I given in (4.1).

Now our computations start. We first compute the interval enclosure $\mathbf{T}$ such that $\tau(q(x^*)) \in \mathbf{T}$ for all $x^* \in I$. The obtained result is

$$\mathbf{T} = [3.058882598, 3.058883224].$$

Next we compute a set B_0 such that (see Figure 10)

$$\psi^{-1}(C^{-1}(q(x^*) - q^0)) \subset B_0.$$

Such a set can be obtained using technical Lemma 9.5 included in the appendix. We thus obtain

$$B_0 = \begin{pmatrix} [-7.91575 \cdot 10^{-12}, 7.91575 \cdot 10^{-12}] \\ [-7.91575 \cdot 10^{-12}, 7.91575 \cdot 10^{-12}] \\ [-9.29424 \cdot 10^{-19}, 9.29424 \cdot 10^{-19}] \\ [-4.50827 \cdot 10^{-8}, 4.50827 \cdot 10^{-8}] \end{pmatrix}.$$

Remark 7.11. *Note that the set is flat along the third coordinate and stretched along the last coordinate. This is because we set up C and ψ so that the third coordinate is associated with the section $\{y = 0\}$ (on which lie $q(x^*)$) and that the last coordinate is associated with the direction of the curve $q(x^*) = (x^*, 0, 0, \kappa(x^*))$.*

We now choose the size of our investigated set B in local coordinates and choose the parameters for our cones (see Figure 10). We take

$$\alpha = 2.56 \cdot 10^{-6}$$

and consider only one branch of the unstable manifold considering

$$B = \bigcup_{v \in B_0} Q^+(v) \cap \{\mathsf{x} \in [\underline{\mathsf{x}}, \overline{\mathsf{x}}]\} \tag{7.15}$$

with

$$\underline{\mathsf{x}} = -1 \cdot 10^{-11}, \qquad \overline{\mathsf{x}} = 4.5 \cdot 10^{-6}.$$

The choice of $\overline{\mathsf{x}}$ is dictated by the size of the fiber we later need to consider to prove intersections of stable/unstable manifolds.

To compute a rigorous enclosure of $[DF(B)]$ using (7.7), we subdivide B into $N = 1200$ parts B_i along the x coordinate

$$B = \bigcup_{i=1}^{N} B_i.$$

Using Lemma 7.3 to obtain enclosures of $F(B_i)$, combined with (7.7) we compute estimates for $[DF(B_i)]$. Combining the estimates $[DF(B_i)]$ we obtain the following global estimate for $[DF(B)]$ (the result is displayed with very rough accuracy, ensuring true enclosure in rounding):

$$[DF(B)] = \begin{pmatrix} [1465.6, 1466.5] & [-0.353, 0.369] & [-0.285, 0.283] & [-0.300, 0.333] \\ [-0.361, 0.360] & [-0.360, 0.361] & [-0.290, 0.277] & [-0.319, 0.304] \\ [-0.138, 0.140] & [-0.139, 0.139] & [0.896, 1.120] & [0.458, 0.700] \\ [-0.201, 0.202] & [-0.202, 0.202] & [-0.171, 0.149] & [0.823, 1.172] \end{pmatrix}.$$

Finally, using $[DF(B)]$ and Lemmas 9.1 and 9.2 (see also Remarks 6.6 and 7.9), we verify the assumptions of Lemma 6.3. We thus obtain rigorous bounds for the position of the fibers. The computation of the enclosure of the fibers took 18 minutes on a single core 2.53 GHz laptop with 4 GB of RAM. For more details on the implementation see section 9.3.

We plot the obtained bounds on fibers transported to the original coordinates of the system x, y, p_x, p_y in Figures 11, 12, and 13. On the plots we present rigorous enclosures of three fibers starting from $q(x^*)$ with x^* on the edges and the middle of interval I (with I chosen in (4.1)). This gives us an overview of the size of our fiber enclosures (left-hand sides of Figures 11, 12, and 13). We can see that close to the set which contains $\{q(x^*) = (x^*, 0, 0, \kappa(x^*)) | x^* \in I\}$, which is depicted in green, the estimates on the fibers are sharp (right-hand plots in Figures 11, 12, and 13). We can see that our three considered fiber enclosures are very close to each other but are still separated, which is visible after a close-up on the left-hand-side plot in Figure 13.

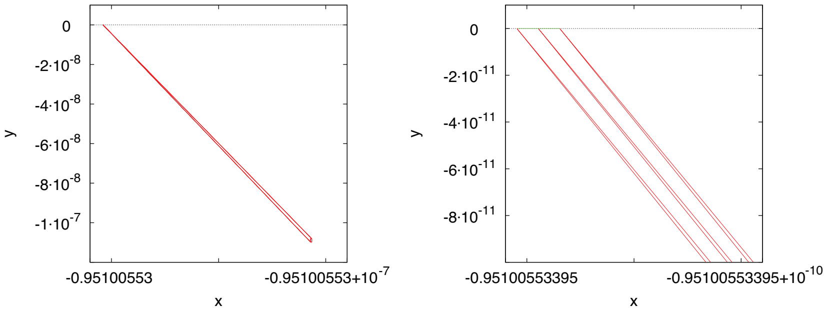

Figure 11. *Projections of fiber enclosures onto x, y coordinates.*

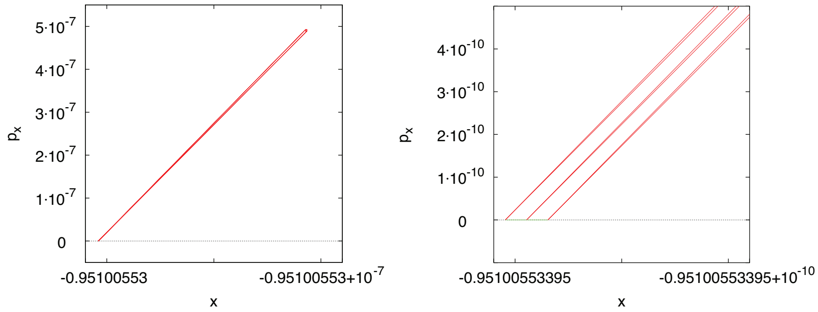

Figure 12. *Projections of fiber enclosures onto x, p_x coordinates.*

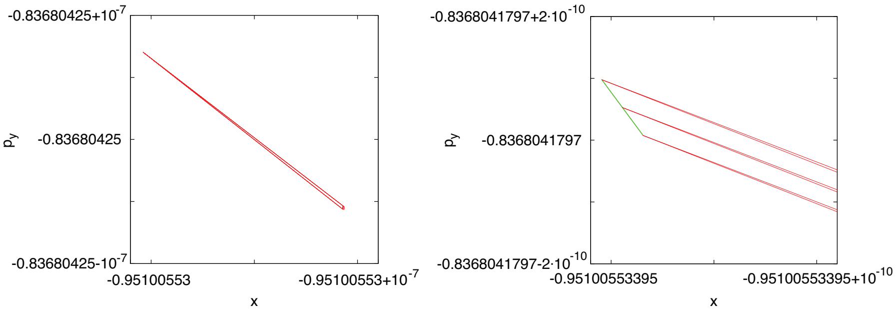

Figure 13. *Projections of fiber enclosures onto x, p_y coordinates.*

Remark 7.12. *The range of obtained fibers is small. It is possible to reach somewhat further from $q(x^*)$, but this significantly increases the time of computation, since further subdivision of the set is required.*

Remark 7.13. *By using linearization only we have not been able to obtain accurate enough enclosure of the fibers to handle the proof of the transversal intersection of manifolds which follows in section 7.4.2. Thus the use of a higher order change of variables seems to be needed.*

7.4.2. Bounds for intersections of manifolds. In this section we present rigorous computer assisted results in which we verify the assumptions of Lemma 7.8 and thus conclude the proof of Theorem 4.1. For each $x^* \in I$ there are four points of intersection of $W^u(L(x^*))$ and

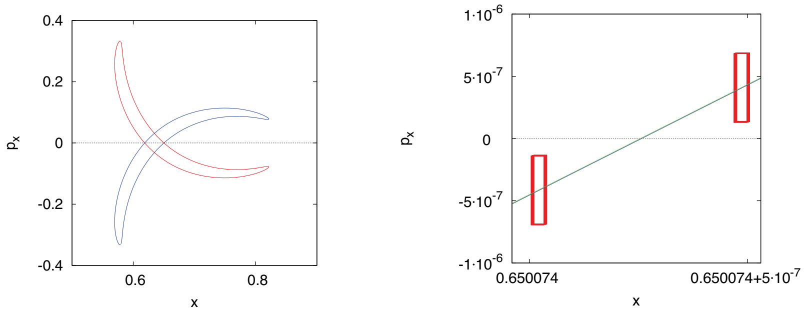

Figure 14. *Left: Numerical sketch of $W^s(L(x^*))$ (in red) and $W^u(L(x^*))$ (in blue) intersected with $\{y=0\}$. Right: The red boxes are the x, p_x projections of $\mathcal{G}(B_E^l)$ (the one over $p_x=0$) and $\mathcal{G}(B_E^r)$ (the one under $p_x=0$). We have proved that $\{\pi_{x,p_x}(W^u(L(x^*))\cap\{y=0\})|x^*\in I\}$ consists of curves passing through the two red boxes. We have also proved that their slope is between* $[1.7695, 1.7725]$. *The blue/green line is a nonrigorous plot of the curves.*

$W^s(L(x^*))$ on $\{y=0\}$. They can be seen in the left-hand plot in Figure 14 (see also Figures 4, 2, and 3). We consider only the rightmost point.

The method presented below exploits the fact that on the point of intersection we have $p_x=0$. This allows for the use of the symmetry of the system in the arguments, which simplifies computation. Similar arguments could be conducted for the points where $p_x\neq 0$. The only difference is that we would need to integrate both along the unstable and stable manifolds. In the following case, when $p_x=0$, it is sufficient to consider the intersection of the unstable manifold with $\{y=0\}$, since the stable manifold follows naturally from symmetry.

We define the set $B_E=\left[\mathsf{x}^l,\mathsf{x}^r\right]\times B_c$ with $\mathsf{x}^l,\mathsf{x}^r$ chosen as

$$\mathsf{x}^m = 4.461867506615821\cdot 10^{-6},$$
$$\mathsf{x}^l=\mathsf{x}^m-10^{-11},\qquad \mathsf{x}^r=\mathsf{x}^m+10^{-11}.$$

We verify that assumption (7.8) of Lemma 7.8 holds by computing $\mathcal{G}(B_E^l)$ and $\mathcal{G}(B_E^r)$. We plot the obtained bounds in red in the right-hand-side plot of Figure 14.

Next, using Remark 7.10, we compute

$$\mathbf{a}=[1.7695, 1.7725]; \tag{7.16}$$

hence assumption (7.9) of Lemma 7.8 holds. Applying Lemma 7.8, we conclude the proof of Theorem 4.1.

We needed to subdivide B_E into 600 parts to compute $[D\mathcal{G}(B_E)V^+]$ and $[D\mathcal{G}(B_E)V^-]$ with sufficient accuracy to obtain (7.16). Verification of assumptions of Lemma 7.8 took 24 minutes on a single core 2.53 GHz laptop with 4 GB of RAM. For more details on the implementation see section 9.3.

Remark 7.14. *From* $\mathbf{a}$ *and by S-symmetry of manifolds $W^u(L(x^*))$ and $W^s(L(x^*))$, we obtain an estimate* $[58.8637^\circ, 58.9439^\circ]$ *on the angle of intersection of the curves on the x,p_x plane.*

Remark 7.15. *In one go we obtain an estimate for a whole family of curves on*

$$\pi_{x,p_x}(W^u(L(x^*))\cap\{y=0\})\quad \textit{for } x^*\in I.$$

In reality these curves are very close to each other (the furthest distance along x^* is about $2.65 \cdot 10^{-9}$). We plotted (using nonrigorous computations) two curves which are furthest from each other on the right-hand-side plot of Figure 14. One is in green and the other in blue. They are visible only after a large magnification and on a paper printout will merge together. This means that our estimate on the position of the curves is somewhat rough in comparison to nonrigorous numerical simulation.

8. Closing remarks and future work.

In this paper we have presented a method for proving existence of families of Lyapunov orbits in the planar circular restricted three body problem (PCR3BP). The method gives explicit bounds on a curve of initial points, which can continue up to half the distance from L_2 to the smaller primary in the Jupiter–Sun system.

We also presented a method of proving transversal intersections of invariant manifolds associated with Lyapunov orbits. The method gives explicit bounds on which the intersection takes place. It has been applied to Lyapunov orbits with the energy of the comet Oterma in the Jupiter–Sun system.

In this paper we have focused on detection of homoclinic intersections. Using identical tools one could also prove heteroclinic intersections of manifolds in the spirit of the work of Wilczak and Zgliczyński [23, 24].

Due to the fact that the presented method gives explicit estimates on the position of investigated manifolds, it is our hope to later apply it to the study of diffusion. Here is an outline of a future scheme that could be followed to prove diffusion. The family of Lyapunov orbits is normally hyperbolic and hence survives time periodic perturbations. In a nonautonomous setting the system no longer preserves energy, which allows for diffusion between orbits of different energies. Such a mechanism has been investigated in [9] for the planar elliptic restricted three body problem, for the system with special restriction on parameters. The discussed diffusion follows from the geometric method of Delshams, de la Llave, and Seara [11, 12, 13] and requires computation of Melnikov-type integrals along homoclinic orbits of the PCR3BP. Since our method allows for precise and rigorous estimates for such orbits, it is our hope that such integrals could be computed using rigorous computer assisted techniques. This combined with topological methods [8, 10] for detection of normally hyperbolic manifolds could give the first rigorous results for diffusion in the three body problem with real-life parameters. From this perspective, the results of this paper are a first step in a larger scheme for investigation of real-life systems.

9. Appendix.

9.1. Verification of cone conditions.

Lemma 9.1. *Let $\mathbf{A}$ be an interval matrix of the form*

$$\mathbf{A} = \begin{pmatrix} \mathbf{a}_{11} & \boldsymbol{\varepsilon}^T \\ \mathbf{B} & \mathbf{C} \end{pmatrix},$$

where $\mathbf{a}_{11} = [\underline{a}_{11}, \overline{a}_{11}]$ with $\underline{a}_{11} > 0$. If, for any $\varepsilon \in \boldsymbol{\varepsilon}$, $\|\varepsilon\| \leq \epsilon$, the inequality

$$\frac{\underline{a}_{11} - \epsilon\sqrt{\alpha}}{\sqrt{1+\alpha}} > m \tag{9.1}$$

holds, then for $v = (\mathsf{x}, \mathsf{y})$ *such that* $Q(v) = \alpha \mathsf{x}^2 - \|\mathsf{y}\|^2 \geq 0$ *and any* $A \in \mathbf{A}$ *we have* $\|Av\| > m\|v\|$.

Proof. For $v = (\mathsf{x}, \mathsf{y})$ satisfying $Q(v) \geq 0$, we have $\|\mathsf{x}\|^2 + \|\mathsf{y}\|^2 \leq \|\mathsf{x}\|^2 (1 + \alpha)$. Using (9.1) this gives the following estimate:

$$\|Av\| \geq \underline{a}_{11}\|\mathsf{x}\| - \epsilon\|\mathsf{y}\| \geq \left(\underline{a}_{11} - \epsilon\sqrt{\alpha}\right)\|\mathsf{x}\| > m\sqrt{\|\mathsf{x}\|^2 + \|\mathsf{y}\|^2} = m\|v\|. \qquad \blacksquare$$

Lemma 9.2. *Let* $Q(v) = Q(\mathsf{x}, \mathsf{y}) = \alpha \mathsf{x}^2 - \|\mathsf{y}\|^2$, *let* C_Q *be a diagonal matrix such that* $v^T C_Q v = Q(v)$, *and let* $\mathbf{A} = [DF(Q^+(v^*))]$. *Assume that* $\mathbf{D} = \mathbf{A^T} C_Q \mathbf{A}$ *is an interval matrix of the form*

$$\mathbf{D} = \begin{pmatrix} \mathbf{d}_{11} & \boldsymbol{\varepsilon}^T \\ \boldsymbol{\varepsilon} & \mathbf{B} \end{pmatrix}.$$

Assume that $\mathbf{d}_{11} = [\underline{d}_{11}, \overline{d}_{11}]$ *with* $\underline{d}_{11} > 0$ *and that for some* $M > 0$, *for any symmetric matrix* $B \in \mathbf{B}$,

$$\inf\{\lambda | \lambda \in \operatorname{spec}(B)\} > -M. \tag{9.2}$$

If for any $\varepsilon \in \boldsymbol{\varepsilon}$ *we have* $\|\varepsilon\| \leq \epsilon$ *and* $\underline{d}_{11} - 2\epsilon > M\alpha$, *then for any* $v_1, v_2 \in U$, $v_1 \neq v_2$ *such that* $Q(v_1 - v_2) \geq 0$

$$Q(F(v_1) - F(v_2)) > 0.$$

Proof. By (6.9) $Q(F(v_1) - F(v_2)) = (v_1 - v_2)^T D(v_1 - v_2)$ for some symmetric matrix $D \in \mathbf{D}$.

For $v = (\mathsf{x}, \mathsf{y})$ such that $Q(\mathsf{x}, \mathsf{y}) \geq 0$ and for any symmetric $D \in \mathbf{D}$,

$$D = \begin{pmatrix} d_{11} & \varepsilon^T \\ \varepsilon & B \end{pmatrix},$$

we compute the following bounds:

$$\begin{aligned} v^T D v &= d_{11}\mathsf{x}^2 + \mathsf{x}\varepsilon^T \mathsf{y} + \mathsf{y}^T \varepsilon \mathsf{x} + \mathsf{y}^T B \mathsf{y} \\ &\geq \underline{d}_{11}\mathsf{x}^2 - 2\epsilon\|\mathsf{y}\||\mathsf{x}| - M\|\mathsf{y}\|^2 \\ &\geq (\underline{d}_{11} - 2\epsilon)\mathsf{x}^2 - M\|\mathsf{y}\|^2 \\ &= M\left(\frac{\underline{d}_{11} - 2\epsilon}{M}\mathsf{x}^2 - \|\mathsf{y}\|^2\right) \\ &> MQ(\mathsf{x}, \mathsf{y}) \\ &> 0. \qquad \blacksquare \end{aligned}$$

Remark 9.3. *Assumption* (9.2) *is easily verifiable from Gershgorin's theorem.*

9.2. Bounds for the images in local coordinates. Here we give a proof of Lemma 7.3.

Proof. Inclusion (7.6) is equivalent to showing that for any $\tau \in \mathbf{T}$ and any $v_1 \in U_1$ there exists a v_2 in U_2 such that

$$G(\tau, v_1, v_2) = 0. \tag{9.3}$$

Let us fix a $\tau \in \mathbf{T}$ and $v_1 \in U_1$ and use the notation $G_{\tau,v_1}(v_2) = G(\tau, v_1, v_2)$. Observe that $[DG_{\tau,v_1}(U_2)] \subset \mathbf{A}(U_2)$ and $[G_{\tau,v_1}(v_0)] \subset [G(\mathbf{T}, U_1, v_0)]$. Since from (7.5)

$$v_0 - [DG_{\tau,v_1}(U_2)]^{-1} G_{\tau,v_1}(v_0) \subset N(\mathbf{T}, v_0, U_1, U_2) \subset U_2,$$

by the interval Newton method (Theorem 2.1) there exists a unique $v_2 = v_2(\tau, v_1) \in U_2$ which satisfies (9.3). ∎

Remark 9.4. *When applying Lemma 7.3, due to very strong hyperbolicity of the map Φ_τ, it pays to use the mean value theorem. Taking $U_1 = v_1 + B$, we can compute*

$$N(\mathbf{T}, v_0, U_1, U_2) = v_0 - [\mathbf{A}(U_2)]^{-1} G(\mathbf{T}, v_1, v_0) - \left[\left(\mathbf{A}(U_2)^{-1} \frac{\partial G}{\partial v_1}(\mathbf{T}, U_1, v_0)\right) B\right].$$

This is a better form since in (below we neglect arguments in order to keep the formula compact)

$$\mathbf{A}^{-1}\frac{\partial G}{\partial v_1} = -D\lambda^{-1} \cdot \left((D\psi)^{-1} \cdot D\tilde{\Phi}_\tau \cdot D\psi\right), \tag{9.4}$$

the strong hyperbolic expansion cancels out. This is the main advantage of Lemma 7.3.

Here we give a technical lemma that can be used for computation of

$$\psi^{-1}(C^{-1}\left((x^*, 0, 0, \kappa(x^*)) - q^0\right)) \quad \text{for } x^* \in I$$

and $q^0 = (x^0, 0, 0, p_y^0)$. Below, R can be any matrix close to $D\psi^{-1}(0)C^{-1}A$.

Lemma 9.5. *Let $a \in \mathbb{R}$ and $J_1 \subset \mathbb{R}$ be from Lemma 3.1, and let*

$$A = \begin{pmatrix} 1 & 0 & 0 & 0 \\ 0 & 1 & 0 & 0 \\ 0 & 0 & 1 & 0 \\ a & 0 & 0 & 1 \end{pmatrix}.$$

Let $\mathbf{B}$ be a set in $\mathbb{R}^4$, let R be a 4×4 matrix, and let

$$M := \left[A^{-1}CD\psi(R\mathbf{B})R\right]^{-1}\left(I - x^0, 0, 0, J_1 - p_y^0\right).$$

If

$$M \subset \mathbf{B}, \tag{9.5}$$

then $\psi^{-1}(C^{-1}((x^*, 0, 0, \kappa(x^*)) - q^0)) \subset R\mathbf{B}$.

Proof. By Lemma 3.1

$$\begin{aligned}(x^*, 0, 0, \kappa(x^*)) &\in (x^0, 0, 0, p_y^0) + \left(I - x^0, 0, 0, a(I - x^0) + J_1 - p_y^0\right) \\ &= q^0 + A\left(I - x^0, 0, 0, J_1 - p_y^0\right);\end{aligned}$$

hence

$$(x^*, 0, 0, \kappa(x^*)) - q^0 \in A\left(I - x^0, 0, 0, J_1 - p_y^0\right). \tag{9.6}$$

Let

$$G_q(p) = A^{-1}C\psi(Rp) - q.$$

If we can show that for any $q \in \left(I - x^0, 0, 0, J_1 - p_y^0\right)$ there exists a $p \in \mathbf{B}$ such that

$$G_q(p) = 0, \tag{9.7}$$

then

$$\psi^{-1}\left(C^{-1}Aq\right) = Rp;$$

hence by (9.6)

$$\psi^{-1}(C^{-1}((x^*, 0, 0, \kappa(x^*)) - q^0)) \subset R\mathbf{B}.$$

To show (9.7) we apply the interval Newton method (Theorem 2.1). Since $\psi(0) = 0$, we can compute

$$\begin{aligned} N(0, \mathbf{B}) &= -\left[\frac{d}{dp}G_q(\mathbf{B})\right]^{-1} G_q(0) \\ &= -\left[A^{-1}CD\psi(R\mathbf{B})R\right]^{-1}(-q) \\ &\subset M, \end{aligned}$$

and by (9.5) combined with Theorem 2.1 we obtain (9.7) and hence obtain our claim. ■

9.3. Details on the computer assisted computations. All the computer assisted proofs have been performed using the Computer Assisted Proofs in Dynamics (CAPD) library available at http://capd.ii.uj.edu.pl.

The proofs of Theorems 3.2 and 4.1 require the

`alglib, dynset, dynsys, interval, map, matrixAlgorithms, poincare, vectalg`

modules from the CAPD library, together with

```
capd/alglib/capd2alglib.h,
capd/matrixAlgorithms/floatMatrixAlgorithms.hpp,
capd/map/CnMap.hpp,
capd/dynsys/CnTaylor.hpp,
capd/poincare/PoincareMap.hpp, and
capd/poincare/TimeMap.hpp
```

header files. All the required fragments of the library are included inside of the `capdtools.h` file, which is the part of the computer assisted proof available at http://wms.mat.agh.edu.pl/~mcapinsk.

All programs are purely serial and have not been parallelized.

Acknowledgments. The author would like to thank Rafael de la Llave for discussions and remarks regarding implementation of the parameterization method. Special thanks go also to Daniel Wilczak for discussions on rigorous computer assisted computations using the CAPD library (http://capd.ii.uj.edu.pl).

The author would also like to express deep and sincere thanks to the anonymous referees for their valuable comments and suggestions, which helped to improve the quality of the paper.

REFERENCES

[1] R. Abraham and J. Marsden, *Foundations of Mechanics*, 2nd ed., Benjamin/Cummings, Advanced Book Program, Reading, MA, 1978.

[2] G. Alefeld, *Inclusion methods for systems of nonlinear equations—the interval Newton method and modifications*, in Topics in Validated Computations (Oldenburg, 1993), Stud. Comput. Math. 5, North–Holland, Amsterdam, 1994, pp. 7–26.

[3] E. Belbruno and B. Marsden, *Resonance hopping in comets*, Astron. J., 113 (1997), pp. 1433–1444.

[4] E. Belbruno, M. Gidea, and F. Topputo, *Weak stability boundary and invariant manifolds*, SIAM J. Appl. Dyn. Syst., 9 (2010), pp. 1061–1089.

[5] E. Belbruno, M. Gidea, and F. Topputo, *Geometry of weak stability boundaries*, Qual. Theory Dyn. Syst., to appear; DOI: 10.1007/s12346-012-0069-x.

[6] R. Broucke, *Periodic Orbits in the Restricted Three–Body Problem with Earth–Moon Masses*, NASA–JPL technical report 32-1168, available online at http://ntrs.nasa.gov/archive/nasa/casi.ntrs.nasa.gov/19680013800_1968013800.pdf, 1968.

[7] X. Cabré, E. Fontich, and R. de la Llave, *The parameterization method for invariant manifolds.* III. *Overview and applications*, J. Differential Equations, 218 (2005), pp. 444–515.

[8] M. J. Capiński and P. Roldán, *Existence of a center manifold in a practical domain around L_1 in the restricted three-body problem*, SIAM J. Appl. Dyn. Syst., 11 (2012), pp. 285–318.

[9] M. J. Capiński and P. Zgliczyński, *Transition tori in the planar restricted elliptic three-body problem*, Nonlinearity, 24 (2011), pp. 1395–1432.

[10] M. J. Capiński and P. Zgliczyński, *Cone conditions and covering relations for topologically normally hyperbolic manifolds*, Discrete Contin. Dyn. Syst., 30 (2011), pp. 641–670.

[11] A. Delshams, R. de la Llave, and T. Seara, *A geometric approach to the existence of orbits with unbounded energy in generic periodic perturbations by a potential of generic geodesic flows of $T2$*, Comm. Math. Phys., 209 (2000), pp. 353–392.

[12] A. Delshams, R. de la Llave, and T. Seara, *A geometric mechanism for diffusion in Hamiltonian systems overcoming the large gap problem: Heuristics and rigorous verification on a model*, Mem. Amer. Math. Soc., 179 (2006), 844.

[13] A. Delshams, R. de la Llave, and T. Seara, *Geometric properties of the scattering map of a normally hyperbolic invariant manifold*, Adv. Math., 217 (2008), pp. 1096–1153.

[14] G. Gómez, À. Jorba, C. Simó, and J. Masdemont, *Dynamics and Mission Design Near Libration Points. Vol.* III. *Advanced Methods for Collinear Points*, World Scientific Monograph Series in Mathematics 4, World Scientific, River Edge, NJ, 2001.

[15] G. Gómez, W. S. Koon, M. W. Lo, J. E. Marsden, J. Masdemont, and S. D. Ross, *Connecting orbits and invariant manifolds in the spatial restricted three-body problem*, Nonlinearity, 17 (2004), pp. 1571–1606.

[16] À. Jorba and C. Simó, *Effective stability for periodically perturbed Hamiltonian systems*, in Hamiltonian Mechanics (Toruń, 1993), NATO Adv. Sci. Inst. Ser. B Phys. 331, Plenum, New York, 1994, pp. 245–252.

[17] À. Jorba and J. Villanueva, *Numerical computation of normal forms around some periodic orbits of the restricted three-body problem*, Phys. D, 114 (1998), pp. 197–229.

[18] W. Koon, M. Lo, J. Marsden, and S. Ross, *Heteroclinic connections between periodic orbits and resonance transitions in celestial mechanics*, Chaos, 10 (2000), pp. 427–469.

[19] J. Llibre, R. Martinez, and C. Simó, *Transversality of the invariant manifolds associated to the Lyapunov family of periodic orbits near L_2 in the restricted three body problem*, J. Differential Equations, 58 (1985), pp. 104–156.

[20] J. Moser, *On the generalization of a theorem of A. Liapounoff*, Comm. Pure Appl. Math., 11 (1958), pp. 257–271.

[21] C. L. Siegel and J. K. Moser, *Lectures on Celestial Mechanics*, Classics in Mathematics, Springer-Verlag, Berlin, 1995.

[22] D. Wilczak and P. Zgliczyński, *Cr-Lohner algorithm*, Schedae Informaticae, 20 (2011), pp. 9–46.

[23] D. Wilczak and P. Zgliczyński, *Heteroclinic connections between periodic orbits in planar restricted circular three body problem—a computer assisted proof*, Comm. Math. Phys., 234 (2003), pp. 37–75.

[24] D. Wilczak and P. Zgliczyński, *Heteroclinic connections between periodic orbits in planar restricted circular three body problem.* II, Comm. Math. Phys., 259 (2005), pp. 561–576.

[25] P. Zgliczyński, *Covering relations, cone conditions and the stable manifold theorem*, J. Differential Equations, 246 (2009), pp. 1774–1819.